phenotype. The BM precursor cells in *Gpr56*$^{-/-}$ mice displayed decreased adhesion to MC3T3-E1 cells, fibronectin, laminin-1 and collagen type III as extracellular matrices (Figure 7a). The ability of BM precursor cells from *Gpr56*$^{-/-}$ mice to migrate towards the chemoattractant stromal cell-derived factor-1 was significantly increased on the three types of coated extracellular matrices (Figure 7b). In the next experiment, we determined the precise localization of HSCs in the BM using confocal microscopy after staining BM sections with phycoerythrin-conjugated c-kit and fluorescein isothiocyanate-conjugated Sca-1 antibodies. The

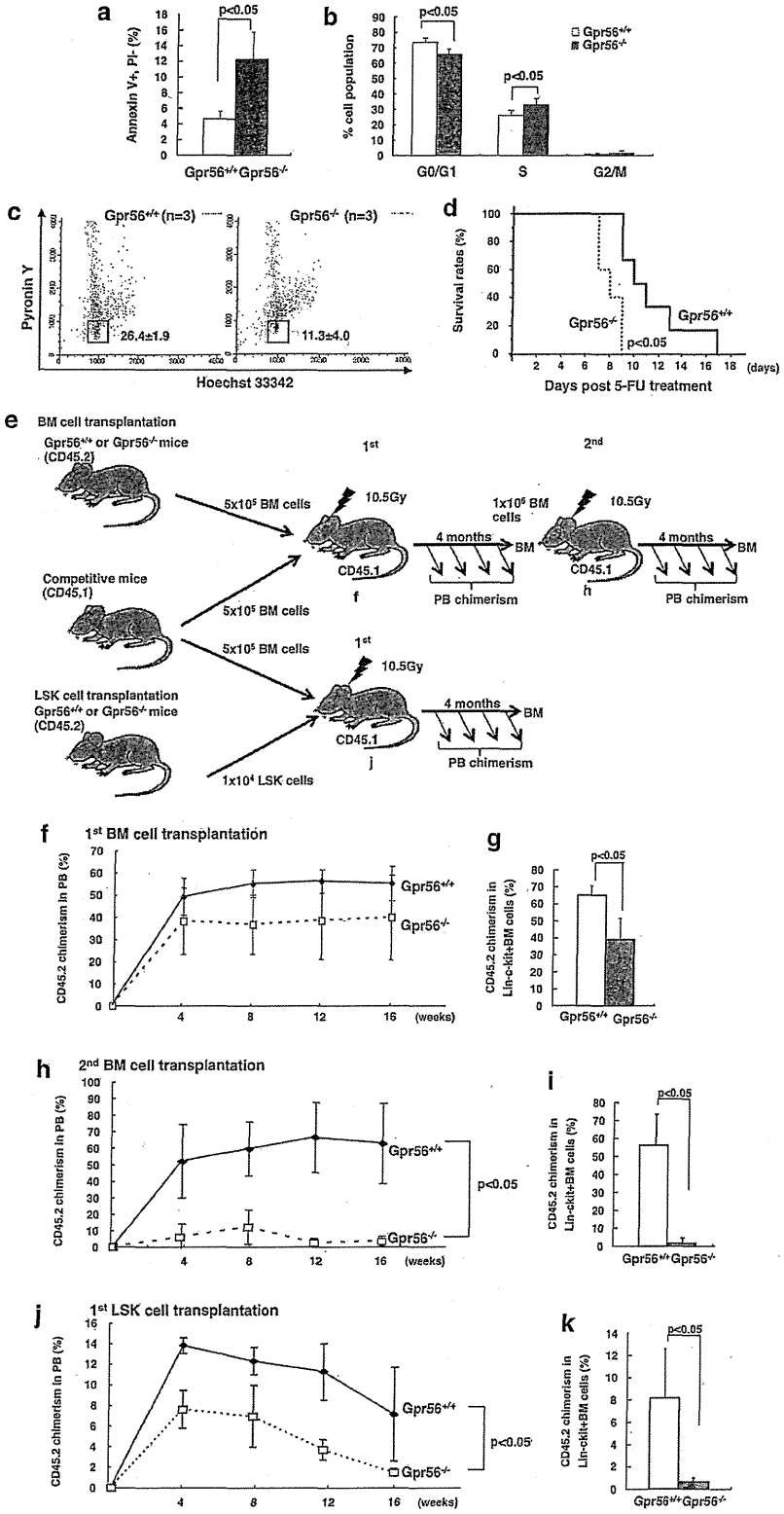

number of primitive cells located less than 20 μm from the periosteum was significantly decreased in the *Gpr56*$^{-/-}$ mice (Figure 7c and Supplementary Figure 10). By contrast, the number of cells that were located more than 50 μm from the periosteum was increased in the *Gpr56*$^{-/-}$ mice. Finally, to investigate whether the migration and adhesion abilities of HSCs depend on GPR56 signaling through the $G\alpha_{12/13}$ and Rho signaling pathway, we determined the protein levels of GTP-bound RhoA in the HSC fractions of wild-type and *Gpr56*$^{-/-}$ mice (Figure 7d). High levels of GTP-bound RhoA accumulated in wild-type mice under both nonstimulated and collagen type III-stimulated conditions, although the stimulation mechanism was unknown in the HSC fraction of wild-type mice. Conversely, low levels of GTP-bound RhoA were detected in the *Gpr56*$^{-/-}$ mice in both the untreated and collagen type III-treated BM cells. In addition, the ability of HSCs to adhere to MC3T3-E1 cells or to fibronectin was significantly decreased by the treatment with Y-27632, a p160ROCK kinase inhibitor (Supplementary Figures 11a and b). Thus, the data suggest that the cellular adhesion of HSCs was decreased by the reduction of RhoA signaling activity, resulting in a reduction in HSCs near the periosteum.

The expression of GPR56 in HSCs was involved in the maintenance of quiescence and long-term BM reconstitution

Because the fraction of LSK cells in *Gpr56*$^{-/-}$ mice was decreased in the BM along with a reduction in their adhesion ability, we next investigated the fraction of apoptotic cells and cell cycle parameters in the LSK fraction in the BM. The Annexin V^{+}7-7-aminoactinomycin D^{-} fraction of apoptotic cells was significantly increased in *Gpr56*$^{-/-}$ mice (Figure 8a and Supplementary Figure 12). The population of G0/G1-phase cells was also decreased, together with an increased population of S-phase cells in the *Gpr56*$^{-/-}$ mice (Figure 8b). Furthermore, the population of G0-phase cells separated by pyronin Y and Hoechst 33342 staining was significantly reduced in the LSK fraction in *Gpr56*$^{-/-}$ mice compared with the population in wild-type mice (Figure 8c). In the next experiment, to determine the drug sensitivity of BM cells in the *Gpr56*$^{-/-}$ mice to an anticancer drug, 5-fluorouracil was injected at a dose of 150 mg/kg once per week for 2 weeks into each of six wild-type and *Gpr56*$^{-/-}$ mice (Figure 8d). The median lifespan of the wild-type mice was 10.5 days, whereas the lifespan of the *Gpr56*$^{-/-}$ mice was significantly shortened to 7.5 days ($P<0.05$); this result suggests that the reduction of the HSC population in the BM and the decreased proportion of G0-phase cells resulted in enhanced cytotoxicity in the *Gpr56*$^{-/-}$ mice in response to this anticancer drug. Finally, to define the ability of HSCs in the *Gpr56*$^{-/-}$ mice to reconstitute hematopoiesis, a mixture of CD45.2^{+} BM cells from wild-type or *Gpr56*$^{-/-}$ mice with CD45.1^{+} competitor BM cells was transplanted into lethally irradiated CD45.1^{+} mice (Figure 8e). In the first transplantation, the population of CD45.2^{+} white blood cells from *Gpr56*$^{-/-}$ mice in the PB was decreased in the recipients compared with the population in the wild-type mice (Figure 8f). Moreover, the population of myeloid, erythroid, megakaryocyte and Lin^{-}c-Kit^{+} BM cells from *Gpr56*$^{-/-}$ mice in the recipient BM was significantly decreased (Figure 8g and Supplementary Figure 13). In the second transplantation, the population of white blood cells from *Gpr56*$^{-/-}$ mice was significantly diminished in the PB and Lin^{-}c-Kit+ BM cell fractions of the recipients (Figures 8h and i).

Furthermore, to confirm the reduced reconstitution ability of the stem cell fraction in the *Gpr56*$^{-/-}$ mice, we transplanted 1×10^{4} LSK cells from wild-type or *Gpr56*$^{-/-}$ mice with CD45.1^{+} competitor BM cells into lethally irradiated CD45.1^{+} mice. As shown in Figures 8j and k, the population of white blood cells from *Gpr56*$^{-/-}$ mice was significantly decreased in the PB and Lin^{-}c-Kit+ BM cell fractions of the recipients. Thus, the reduction of cell numbers and the depletion of the quiescent cell population in BM-derived HSCs may result in a reduced capacity for HSC reconstitution in *Gpr56*$^{-/-}$ mice.

DISCUSSION

In this study, RhoA signaling through $G\alpha_{12/13}$ coupled with GPR56 is a novel signaling pathway for HSC maintenance in BM, which is regulated by EVI1. As high levels of GPR56 expression correlate with the cellular transformation phenotypes of several cancer tissues,[21–23] high expression of GPR56 in EVI1^{high} AML cells may result in apoptotic resistance with a poor prognosis.

Rac1/Rac2 and the Rho family GTPase Cdc42 previously have been implicated in the maintenance of HSCs through the regulation of adhesion, migration, homing and mobilization. HSCs from Cdc42-deficient mice exhibit impaired adhesion, homing, lodging and retention, leading to massive cellular egress from the BM to distal organs and PB, ultimately resulting in failure of engraftment.[25,29] Rac-1-deficient HSCs show a significant reduction in hematopoietic reconstitution, without any effect on cellular adhesion. However, Rac2-deficient HSCs exhibit decreased cellular adhesion but normal short-term engraftment, suggesting a prominent role for Rac2 in integrin-mediated stem cell adhesion.[26–28] On the other hand, P190-B RhoGAP is a major regulator of Rho GTPases, and abnormally high levels of active RhoA protein were detected in embryo-derived cells from P190-B-deficient mice. The migration and adhesion of hematopoietic progenitor cells from the P190-deficient mice were markedly enhanced in an *in vitro* experiment, and the high levels of active RhoA were associated with a significant enhancement of HSC engraftment and reconstitution *in vivo*.[32] In this study, we demonstrated that downregulation of GPR56 expression in EVI1^{high} leukemia cells and *Gpr56*$^{-/-}$ LSK cells caused RhoA inactivation with a concomitant decrease in cellular adhesion. Moreover, apoptotic cell death and decreased G0 cell fractions in leukemia cells and HSC cells with low RhoA activity were found in both *in vitro* and *in vivo* experiments, and the inactivation of RhoA activity in HSC cells from *Gpr56*-deficient mice reduced the reconstitution ability. On the basis of the findings of P190-B- and GPR56-deficient mice, the level of RhoA activation may significantly influence the maintenance of the HSCs in BM.

Rac is activated by the stimulation of CXCR4 by stromal cell-derived factor-1, by adhesion via β1 integrin, and by the stimulation of c-Kit by stem cell factors, all of which are involved in stem cell engraftment. However, no specific ligands of GPR56 other than collagen type III are currently known. Because the expression level of GPR56 was significantly higher in CD34^{+} CD38^{-}EVI1^{high} LSC fractions than in normal HSCs (Supplementary Figure 14), GPR56 has the potential to become a novel molecular target in EVI1^{high} leukemia. The results of this study have led to a significant improvement in our understanding of stem cell retention in BM and trafficking in the peripheral circulation. Furthermore, if the specific ligand of GPR56 is identified, we will be able to develop a small-molecule inhibitor or antibody as a specific therapeutic target for refractory leukemia that could modulate the adhesion, mobilization and proliferation abilities of EVI1^{high} leukemia cells.

CONFLICT OF INTEREST

The authors declare no conflict of interest.

ACKNOWLEDGEMENTS

We gratefully acknowledge Genentech for providing the *Gpr56* knockout mice for the studies. This work was supported by a grant-in-aid for the third term comprehensive 10-year strategy for cancer control from the Ministry of Health and Welfare; a grant-in-aid for scientific research from The Ministry of Education, Culture, Sports, Science and Technology; a grant-in-aid for scientific research from the Japan Society for the Promotion of Science; and a Grant-in-Aid for Scientific Research on Innovative Areas.

REFERENCES

1 Ishikawa F, Yoshida S, Saito Y, Hijikata A, Kitamura H, Tanaka S *et al.* Chemotherapy-resistant human AML stem cells home to and engraft within the bone-marrow endosteal region. *Nat Biotechnol* 2007; **25**: 1315–1321.

2 Lane SW, Scadden DT, Gilliland DG. The leukemic stem cell niche: current concepts and therapeutic opportunities. *Blood* 2009; **114**: 1150–1157.

3 Morishita K, Parker DS, Mucenski ML, Jenkins NA, Copeland NG, Ihle JN. Retroviral activation of a novel gene encoding a zinc finger protein in IL-3-dependent myeloid leukemia cell lines. *Cell* 1988; **54**: 831–840.

4 Morishita K, Parganas E, William CL, Whittaker MH, Drabkin H, Oval J *et al.* Activation of EVI1 gene expression in human acute myelogenous leukemias by translocations spanning 300–400 kilobases on chromosome band 3q26. *Proc Natl Acad Sci USA.* 1992; **89**: 3937–3941.

5 Lugthart S, Gröschel S, Beverloo HB, Kayser S, Valk PJ, van Zelderen-Bhola SL *et al.* Clinical, molecular, and prognostic significance of WHO type inv(3)(q21q26.2)/t(3;3)(q21;q26.2) and various other 3q abnormalities in acute myeloid leukemia. *J Clin Oncol* 2010; **28**: 3890–3898.

6 Barjesteh van Waalwijk van Doorn-Khosrovani S, Erpelinck C, van Putten WL, Valk PJ, van der Poel-van de Luytgaarde S, Hack R *et al.* High EVI1 expression predicts poor survival in acute myeloid leukemia: a study of 319 *de novo* AML patients. *Blood* 2003; **101**: 837–845.

7 Lugthart S, van Drunen E, van Norden Y, van Hoven A, Erpelinck CA, Valk PJ *et al.* High EVI1 levels predict adverse outcome in acute myeloid leukemia: prevalence of EVI1 overexpression and chromosome 3q26 abnormalities underestimated. *Blood* 2008; **111**: 4329–4337.

8 Groschel S, Lugthart S, Schlenk RF, Valk PJ, Eiwen K, Goudswaard C *et al.* High EVI1 expression predicts outcome in younger adult patients with acute myeloid leukemia and is associated with distinct cytogenetic abnormalities. *J Clin Oncol* 2010; **28**: 2101–2107.

9 Valk PJ, Verhaak RG, Beijen MA, Erpelinck CA, Barjesteh van Waalwijk van Doorn-Khosrovani S, Boer JM *et al.* Prognostically useful gene-expression profiles in acute myeloid leukemia. *N Engl J Med* 2004; **350**: 1617–1628.

10 Verhaak RG, Wouters BJ, Erpelinck CA, Abbas S, Beverloo HB, Lugthart S *et al.* Prediction of molecular subtype in acute myeloid leukemia based on gene expression profiling. *Haematologica* 2009; **94**: 131–134.

11 Eppert K, Takenaka K, Lechman ER, Waldron L, Nilsson B, van Galen P *et al.* Stem cell gene expression programs influence clinical outcome in human leukemia. *Nat Med* 2011; **17**: 1086–1093.

12 Yuasa H, Oike Y, Iwama A, Nishikata I, Sugiyama D, Perkins A *et al.* Oncogenic transcription factor Evi1 regulates hematopoietic stem cell proliferation through GATA-2 expression. *EMBO J.* 2005; **24**: 1976–1987.

13 Goyama S, Yamamoto G, Shimabe M, Sato T, Ichikawa M, Ogawa S *et al.* Evi-1 is a critical regulator for hematopoietic stem cells and transformed leukemic cells. *Cell Stem Cell* 2008; **3**: 207–220.

14 Saito Y, Nakahata S, Yamakawa N, Kaneda K, Ichihara E, Suekane A *et al.* CD52 as a molecular target for immunotherapy to treat acute myeloid leukemia with high EVI1 expression. *Leukemia* 2011; **25**: 921–931.

15 Yamakawa N, Kaneda K, Saito Y, Ichihara E, Morishita K. The increased expression of integrin a6 (ITGA6) enhances drug resistance in EVI1high leukemia. *PLoS ONE* 2012; **7**: e30706.

16 Ichihara E, Kaneda K, Saito Y, Yamakawa N, Morishita K. Angiopoietin1 contributes to the maintenance of cell quiescence in EVI1high leukemia cells. *BBRC* 2011; **416**: 239–245.

17 Piao X, Hill RS, Bodell A, Chang BS, Basel-Vanagaite L, Straussberg R *et al.* G protein-coupled receptor-dependent development of human frontal cortex. *Science* 2004; **303**: 2033–2036.

18 Li S, Jin Z, Koirala S, Bu L, Xu L, Hynes RO *et al.* GPR56 regulates pial basement membrane integrity and cortical lamination. *J Neurosci* 2008; **28**: 5817–5826.

19 Koirala S, Jin Z, Piao X, Corfas G. GPR56-regulated granule cell adhesion is essential for rostral cerebellar development. *J Neurosci* 2009; **29**: 7439–7449.

20 Iguchi T, Sakata K, Yoshizaki K, Tago K, Mizuno N, Itoh H. Orphan G protein-coupled receptor GPR56 regulates neural progenitor cell migration via a G alpha 12/13 and Rho pathway. *J Biol Chem* 2008; **283**: 14469–14478.

21 Shashidhar S, Lorente G, Nagavarapu U, Nelson A, Kuo J, Cummins J *et al.* GPR56 is a GPCR that is overexpressed in gliomas and functions in tumor cell adhesion. *Oncogene* 2005; **24**: 1673–1682.

22 Xu L, Begum S, Hearn JD, Hynes RO. GPR56, an atypical G protein-coupled receptor, binds tissue transglutaminase, TG2, and inhibits melanoma tumor growth and metastasis. *Proc Natl Acad Sci USA* 2006; **103**: 9023–9028.

23 Ke N, Sundaram R, Liu G, Chionis J, Fan W, Rogers C *et al.* Orphan G protein-coupled receptor GPR56 plays a role in cell transformation and tumorigenesis involving the cell adhesion pathway. *Mol Cancer Ther* 2007; **6**: 1840–1850.

24 Terskikh AV, Easterday MC, Li L, Hood L, Kornblum HI, Geschwind DH *et al.* From hematopoiesis to neuropoiesis: evidence of overlapping genetic programs. *Proc Natl Acad Sci USA* 2001; **98**: 7934–7939.

25 Yang FC, Atkinson SJ, Gu Y, Borneo JB, Roberts AW, Zheng Y *et al.* Rac and Cdc42 GTPases control hematopoietic stem cell shape, adhesion, migration, and mobilization. *Proc Natl Acad Sci USA* 2001; **98**: 5614–5618.

26 Cancelas JA, Lee AW, Prabhakar R, Stringer KF, Zheng Y, Williams DA. Rac GTPases differentially integrate signals regulating hematopoietic stem cell localization. *Nat Med* 2005; **11**: 886–891.

27 Gu Y, Filippi MD, Cancelas JA, Siefring JE, Williams EP, Jasti AC *et al.* Hematopoietic cell regulation by Rac1 and Rac2 guanosine triphosphatases. *Science* 2003; **302**: 445–449.

28 Ghiaur G, Lee A, Bailey J, Cancelas JA, Zheng Y, Williams DA. Inhibition of RhoA GTPase activity enhances hematopoietic stem and progenitor cell proliferation and engraftment. *Blood* 2006; **108**: 2087–2094.

29 Yang L, Wang L, Geiger H, Cancelas JA, Mo J, Zheng Y. Rho GTPase Cdc42 coordinates hematopoietic stem cell quiescence and niche interaction in the bone marrow. *Proc Natl Acad Sci USA* 2007; **104**: 5091–5096.

30 Ghiaur G, Ferkowicz MJ, Milsom MD, Bailey J, Witte D, Cancelas JA *et al.* Rac1 is essential for intraembryonic hematopoiesis and for the initial seeding of fetal liver with definitive hematopoietic progenitor cells. *Blood* 2008; **111**: 3313–3321.

31 Luo R, Jeong SJ, Jin Z, Strokes N, Li S, Piao X. G protein-coupled receptor 56 and collagen III, a receptor-ligand pair, regulates cortical development and lamination. *Proc Natl Acad Sci USA* 2011; **108**: 12925–12930.

32 Xu H, Eleswarapu S, Geiger H, Szczur K, Daria D, Zheng Y *et al.* Loss of Rho GTPase activating protein p190-B enhances hematopoietic stem cell engraftment potential. *Blood* 2009; **114**: 3557–3566.

Supplementary Information accompanies this paper on the Leukemia website (http://www.nature.com/leu)

Cell Biology International ISSN 1065-6995
doi: 10.1002/cbin.10101

SHORT COMMUNICATION

Genistein induces apoptotic cell death associated with inhibition of the NF-κB pathway in adult T-cell leukemia cells

Masao Yamasaki[1], Yoshihiro Mine[1], Misato Nishimura[1], Satoshi Fujita[1], Yoichi Sakakibara[1], Masahito Suiko[1], Kazuhiro Morishita[2] and Kazuo Nishiyama[1]*

1 Faculty of Agriculture, Department of Biochemistry and Applied Biosciences, University of Miyazaki, 1-1 Gakuenkibanadai-nishi, Miyazaki 889-2192, Japan
2 Faculty of Medicine, Department of Biochemistry, University of Miyazaki, 5200 Kihara Kiyotake, Miyazaki 889-1692, Japan

Abstract

We have shown that genistein inhibits the growth of adult T-cell leukemia (ATL) cells in vitro and in vivo, and this leads to pronounced G2/M arrest. This report shows that genistein induces apoptotic death in ATL cells. Although the pan-caspase inhibitor, Z-VAD-fmk, did not inhibit genistein-induced apoptosis, release of apoptosis-inducing factor (AIF) into the cytosol occurred. Poly-ADP ribose polymerase inhibition also abrogated genistein-induced apoptosis. Genistein decreased nuclear p65 translocation and IκBα phosphorylation, and downregulated the anti-apoptotic proteins, XIAP, cIAP and survivin, NF-κB-responsive gene products. Thus, genistein is a promising agent for ATL that induces caspase-independent apoptosis through inhibition of the NF-κB pathway.

Keywords: adult T-cell leukemia; apoptosis inducing factor; caspase; genistein; isoflavone; NF-κB pathway

Introduction

Southwestern Kyushu in Japan is known for its high prevalence of human T-lymphotropic virus type I (HTLV-I). HTLV-I is the etiologic agent of the $CD4^+$ T-cell malignancy adult T-cell leukemia (ATL). Therefore, ATL is designated as an endemic disease particularly in certain pockets of the Japanese population. Among infected individuals, only 1–5% develop ATL, and it is well established that this process requires 20–50 years after HTLV-I infection. ATL is categorised into four types according to its clinical phenotypes: acute, chronic, smoldering and lymphoma. The acute type constitutes 55–75% of all ATL cases (Hanchard et al., 1990; Yamaguchi et al., 1990). Acute ATL is aggressively malignant and fatal, as it is accompanied by pulmonary complications, opportunistic infections and uncontrolled hypercalcemia. Aggressive forms of ATL are resistant to conventional chemotherapy. Therefore, it is important to identify appropriate therapeutic methods to prevent the development of ATL or prolong survival after its occurrence.

Local cofactors, such as food culture, play an important role in ATL occurrence. In Japan in particular, ATL develops ~50 years after infection, which is comparatively longer than in other areas of the world. Some components from natural foods, for example as curcumin, capsaicin and fucoidan, are effective in ATL treatment (Zhang et al., 2003; Haneji et al., 2005; Tomita et al., 2006a, b). Soybean isoflavone inhibits the proliferation or induces cell death in different types of cancers, including those involving non-ATL leukemia cells (Hewitt and Singletary, 2003; Su et al., 2003; Chang et al., 2004; Liao et al., 2004). We previously showed that soy isoflavones potently inhibited the proliferation of ATL cells in vitro and in vivo (Yamasaki et al., 2007). Genistein demonstrated a striking ability to induce the accumulation of p53 protein and stimulate its phosphorylation at ser-15, 20 and 37 in ATL cells. This effect was accompanied by growth inhibition and G2/M arrest. Genistein also induced cell death in ATL cells, but the molecular mechanisms remain unclear. Here, we have examined the apoptosis inducing activity and role of the NF-κB pathway in the cytotoxic effect of genistein on ATL cells.

***Corresponding author:** e-mail: nishiyam@cc.miyazaki-u.ac.jp
Abbreviations: HTLV-I, human T-lymphotropic virus type I; ATL, adult T-cell leukemia; TSP/HAM, tropical spastic paraparesis/HTLV-I-associated myelopathy; TTBS, Tris-buffered saline with 0.1% Tween-20; PBS, phosphate-buffered saline; PFT, pifithrin-α; 3-AB, 3-aminobenzamide; PARP, poly-ADP ribose polymerase; AIF, apoptosis-inducing factor; cIAP-2, cellular inhibitor of apoptosis protein-2; XIAP, X-linked inhibitor of apoptosis protein

Materials and methods

Materials

Genistein was obtained from Fujicco (Kobe, Japan). 3-Aminobenzamide (3-AB) (Enzo Life Sciences), Z-VAD-fmk (Peptide Institute, Osaka, Japan) and Bay11-7082 (Cayman Chemical, Ann Arbor, MI) were used to inhibit poly-ADP ribose polymerase (PARP), pan-caspase and IκB-α respectively. Peroxidase-conjugated anti-mouse IgG, peroxidase-conjugated anti-rabbit IgG and anti-COX4 were obtained from Santa Cruz Biotechnology, Santa Cruz, CA). Anti-β-actin clone AC-15 was obtained from Sigma (St. Louis, MO); anti-histone H1 was obtained from Acris Antibodies (Herford, Germany), and other antibodies (against NF-κB p65, phosphorylated IκBα, IκBα, apoptosis-inducing factor (AIF), cellular inhibitor of apoptosis protein-2 (cIAP-2), X-linked inhibitor of apoptosis protein (XIAP) and survivin were purchased from Cell Signaling Technology (Beverly, MA).

Cell culture

Hut102 cells provided by Hayashibara Biochemical Laboratories, Inc. (Okayama, Japan) were maintained in RPMI1640 medium supplemented with 10% fetal bovine serum containing 100 units/mL penicillin G and 100 μg/mL streptomycin. The cells were subcultured twice a week. For experiments, the cells were adjusted to 1×10^5 per mL and cultured with 0–30 μM isoflavones for 24 and 48 h.

Cell cycle analysis

The cells were fixed in ice-cold methanol for 30 min before treatment with 10 μg/mL propidium iodide and 10 μg/mL RNase. Cycle analysis involved a Coulter, Epics XL flow cytometer (Beckman Coulter, Inc., Fullerton, CA) equipped with MultiCycle software (San Diego, CA).

Annexin-V staining

Annexin-V positive cells were identified using a commercial kit (Bender MedSystems, Vienna, Austria). After staining, the ratio of annexin-V positive cells among all cells was detected by flow cytometry.

Western blot analysis

At the end of the culture period, cells were lysed in 50 mM Tris–HCl (pH 7.5) containing 150 mM NaCl, 2% Triton X-100, 2 mM EDTA, 50 mM NaF, 30 mM $Na_4P_2O_7$ and 1/50 volume protease inhibitor cocktail (NacalaiTesque, Kyoto, Japan) for the analysis of total cell lysate. Nuclear and cytoplasmic extracts was separated and prepared using the NE-PER Nuclear and Cytoplasmic Extraction Reagents (Pierce, Rockford, IL). For the detection of cytosolic AIF, cells were treated with ice-cold cytosol recovery buffer (0.025% digitonin, 5 mM $MgCl_2$, 1 mM EDTA, 10 mM KCl, 250 mM sucrose, 25 mM NaF, 1 mM sodium orthovanadate/20 mM HEPES-KOH at pH 7.2) for 5 min. After centrifugation at 8,500*g* for 5 min, the supernatant was used as cytosolic fraction. Protein concentration was measured using the BCA protein assay reagent (Pierce). Lysates containing 10 μg of protein were separated by electrophoresis on a 10% SDS–polyacrylamide gel and transferred to PVDF Hybond-P membrane (Amersham-Pharmacia Biotech, Buckinghamshire, UK). Blocking used 5% defatted milk or 5% bovine serum albumin fraction V (for the detection of phosphorylated protein) in Tris-buffered saline with 0.1% Tween-20 (TTBS). Antibodies were diluted in Can Get Signal solutions 1 and 2 (Toyobo, Tokyo, Japan). The membrane was washed with TTBS after each antibody binding reaction. Detection of each protein was performed using the ECL Plus kit (Amersham Pharmacia). The band intensity was quantified using the Image J software and data shown are representative blot patterns. Mean values were determined for at least three independent experiments.

Statistical analysis

Data were analysed using Student's *t*-test and the Tukey–Kramer test to evaluate the significance of differences. Significance was defined as $P < 0.05$.

Results

Genistein inhibits growth and induces apoptosis of ATL cells

Genistein strongly inhibited the growth of ATL cells in vitro and in vivo, as previously known (Figure 1A). In particular, 30 μM genistein completely inhibited the growth of Hut102 cells at 24, 48 and 72 h, inducing the accumulation of the G2/M population (Figure 1B). At 10 μM, genistein significantly inhibited growth at 48 and 72 h, but did not increase the G2/M phase population. Genistein (30 μM) significantly increased the su-G1 population and annexin V-positive cells at 48 h (Figures 1B and 1C), which suggest that cell cycle arrest and the induction of apoptotic cell death both contributed to the growth inhibition of ATL cells. The mitochondrial membrane potential was strongly impaired at 30 μM treatment, but not by 10 μM t at 24 and 48 h (Figure 1D).

Genistein induces caspase-independent apoptosis

To determine the molecular mechanism underlying genistein-induced apoptosis, cells were treated with Z-VAD-fmk

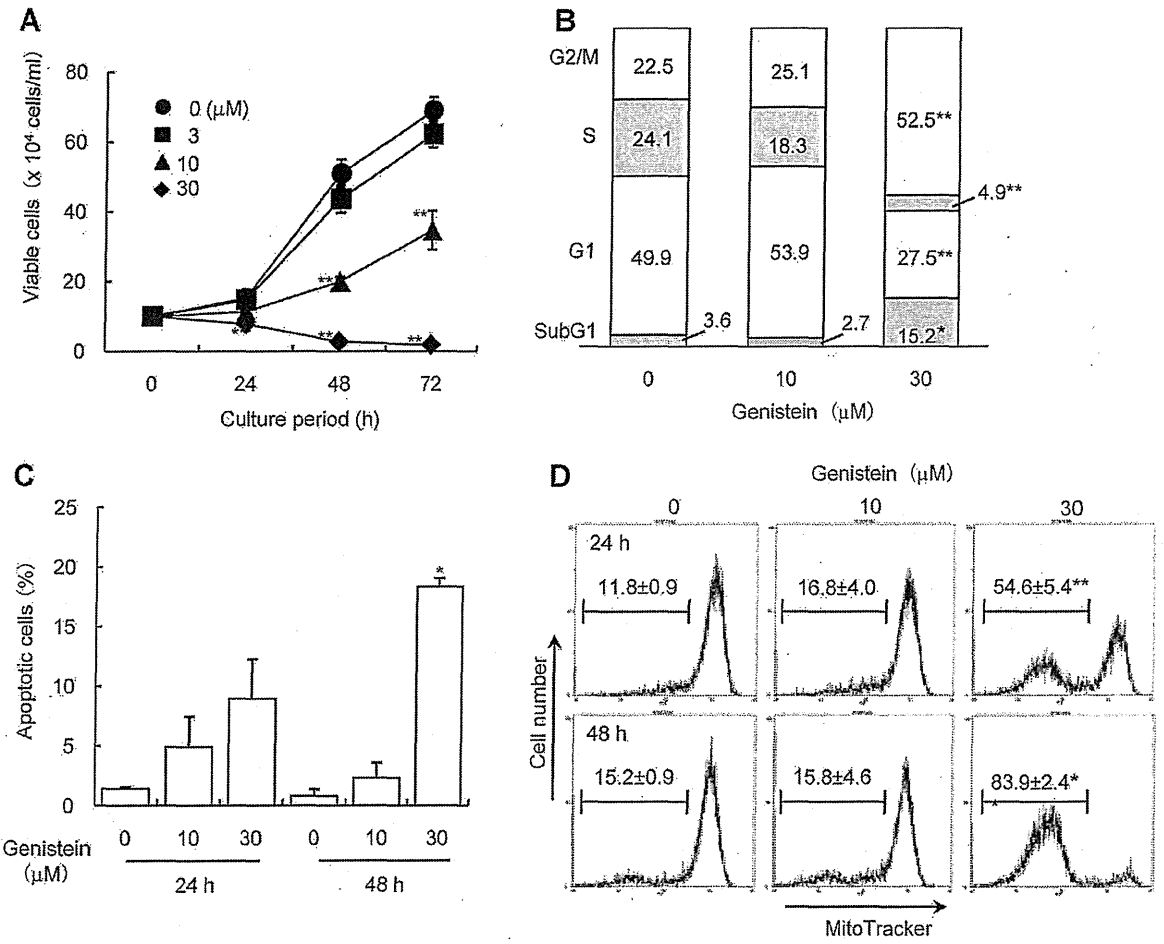

Figure 1 Induction of apoptotic cell death and G2/M cell cycle arrest of Hut102 cells by genistein. (A) Cells were treated with 0, 3, 10 and 30 μM genistein for 24–72 h and viable cells were counted using the trypan blue dye exclusion method. (B) Cells were treated with 0, 10 and 30 μM genistein for 48 h and cell cycle analysis was performed. (C,D) Cells were treated with 0, 10 and 30 μM genistein for 24 or 48 h and the number of Annexin-V-positive cells (C) and the mitochondria membrane potential (D) were determined by flow cytometry. Data are shown as the mean ± SE of three independent experiments. Bars marked with asterisks are significant with respect to the control at $^*P < 0.05$ and $^{**}0.01$.

to assess the involvement of a caspase-dependent pathway. Z-VAD-fmk had no effect on the number of viable cells (Figure 2A). Western blot analysis showed that genistein did not activate caspase-3 (data not shown), which implies the involvement of a caspase-independent pathway. Cytosolic AIF levels were increased by 30 μM genistein treatment for 24 h (Figure 2B). COX4, a mitochondrial marker protein, was not detected in cytosolic fraction, showing no contamination of mitochondrial protein into cytosolic fraction (Figure 2C). AIF release from mitochondria is known to be stimulated by poly-ADP ribose which is a product of PARP overactivation. Thus, the cells treated with 3-AB, inhibitor of PARP, and genistein showed that the former partially abrogated the cytotoxic activity of the latter (Figure 2D).

Genistein decreases NF-κB activity

Finally, the effect of genistein on the activity of NF-κB was examined. Although 30 μM genistein significantly reduced the number of viable cells and impaired the mitochondrial membrane potential after 24 h of treatment, nuclear p65 and phosphorylated IκBα levels were unchanged. However, the levels of nuclear p65 and phosphorylated IκBα decreased significantly after 48 h (Figure 3A). GAPDH was not detected in nuclear fraction, and a strong signal of histone H1 expression was detected in nuclear fraction (Figure 3B), showing no contamination of cytosol protein into nuclear fraction. Although this data indicate that cytosolic fraction contains histone H1, we did not use cytosolic fraction for analysis. NF-κB mediates the

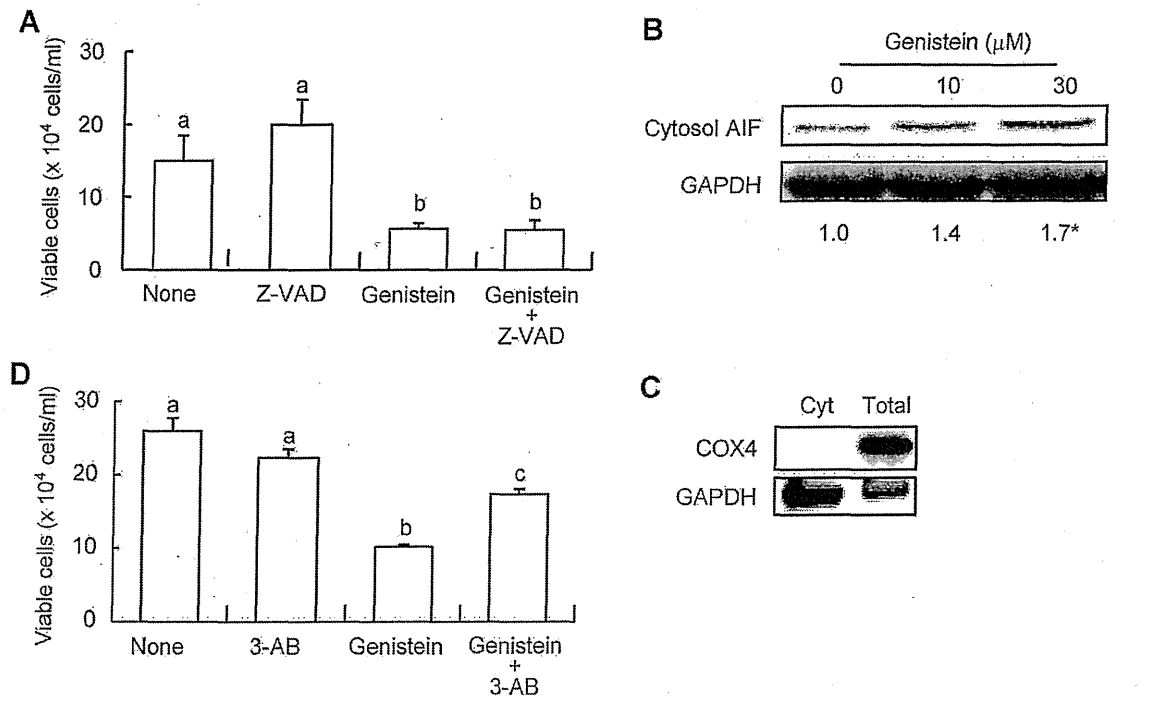

Figure 2 *Genistein induces caspase independent apoptosis.* (A,C) *Cells were treated with 0 and 30 μM genistein with 0 and 20 μM Z-VAD-fmk* (A) or 0 and 20 mM 3-AB (D) for 24 h and viable cells were counted using the trypan blue dye exclusion method. (A) Cells were treated with 0, 10 and 30 μM genistein for 24 h, and cytosolic AIF and GAPDH were then detected using Western blot analysis. Data in (A) and (D) are shown as means ± SE of three independent experiments and the numbers in (B) show the mean values of the quantified band intensities for three independent experiments. The representative blot patterns are shown. Numbers marked with asterisks are significant with respect to the control at $^{*}P < 0.05$ and $^{**}0.01$. Values that do not sharing any alphabetic letters are significantly different from each other, $P < 0.05$. (C) COX4 and GAPDH detection in cytosolic fraction to confirm no contamination between subcellular fractions. Cyt, cytosolic fraction.

transcription of several anti-apoptotic proteins (Figure 3C). Bay11-7082 was used as a positive control for NF-κB inhibition. After 48 h treatment with 10 and 30 μM genistein, the levels of cIAP-2, XIAP and survivin were significantly decreased.

Discussion

Having shown that genistein strongly inhibits the growth of ATL cells in vitro and in vivo via G2/M cell cycle arrest (Figures 1A and 1B), we found that 30 μM genistein significantly increased the sub-G1 population and the number of annexin V-positive cells, suggesting that cell cycle arrest and induction of apoptotic cell death both contribute to the growth inhibition of ATL cells. In contrast to extrinsic death signals, cellular stresses (DNA damage) induce an intrinsic apoptotic program regulated predominantly by the mitochondria. Because these stimuli induce permeabilisation of the mitochondrial outer membrane, the findings in Figures 1B–D suggest that genistein-induced mitochondria-mediated apoptosis in Hut102 cells. Soy-bean isoflavone induced apoptotic cell death in xenografted ATL cells in non-obese diabetic/SCID/gammac null (NOG) mice (Yamasaki et al., 2007). Thus, mitochondria-mediated apoptotic cell death may be involved in the growth inhibitory effect of genistein on ATL cells.

Genistein can induce apoptotic cell death in different types of cells (Hewitt and Singletary, 2003; Su et al., 2003; Chang et al., 2004; Liao et al., 2004). It also induces caspase-dependent apoptosis in ALL, multiple myeloma cells and T-lymphoma cells (Baxa et al., 2005; Li et al., 2011). In contrast, our data show that caspase activation is dispensable for cell death, suggesting the importance of other apoptotic pathways. AIF is a caspase-independent death effect that is localised to the mitochondria under steady-state conditions, but translocates to the cytosol and nucleus under different apoptotic stimuli, including genistein administration (Karmakar et al., 2009; Mohan et al., 2009). Genistein induces translocation of AIF to the cytosolic fraction, which implies that AIF-mediated apoptotic cell death. PARP-1 activation and the resulting poly-ADP ribose (PAR) overproduction promotes to AIF translocation from mitochondria to nuclei (Yu et al., 2002, 2006). The PARP inhibitor, 3-AB, partially abrogated the cytotoxicity of

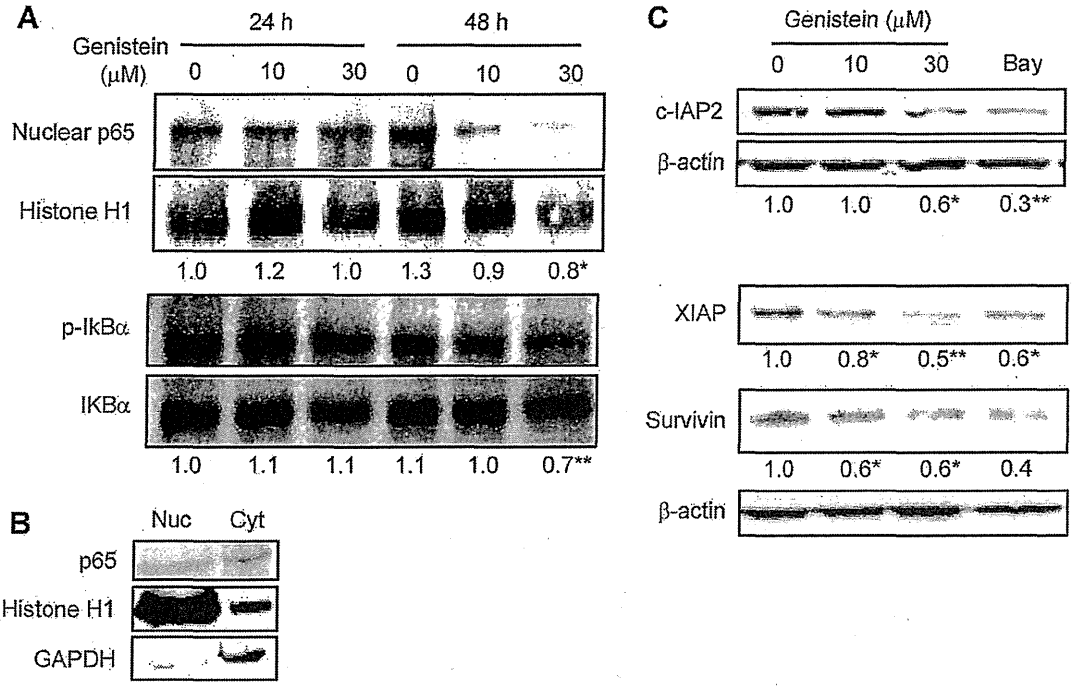

Figure 3 *Genistein ameliorates overactivation of the NF-κB pathway.* (A) Cells were treated with 0, 10 and 30 μM genistein for 24 and 48 h, and nuclear p65, histone H1, phosphorylated IκBα (p-IκBα) and β-actin were detected using Western blot analysis. (C) Cells were treated with 0, 10 and 30 μM genistein or 1 μM Bay11-7082 (Bay) for 48 h, and then c-IAP2, XIAP, survivin and β-actin were detected using Western blot analysis. Numbers represent the mean values of the quantified band intensities for three independent experiments. Representative blot patterns are shown. Numbers marked with asterisks are significant with respect to the control at $^*P < 0.05$ and $^{**}0.01$. (B) p65, histone H1 and GAPDH detection in cytosolic and nuclear fraction to confirm no contamination between subcellular fractions. Nuc, nuclear fraction; Cyt, cytosolic fraction.

genistein, which suggests that PARP activation and the resulting AIF-mediated apoptosis at least partially contribute to the cytotoxicity of genistein.

The HTLV-I viral protein, Tax, activates the expression of several genes through NF-κB, which results in deregulated cell proliferation and resistance to apoptosis (Taylor and Nicot, 2008; Saggioro et al., 2009). XIAP and surviving, which are anti-apoptotic proteins, and NF-κB responsive genes are abundantly expressed in HTLV-1-infected T-cell lines (Mori et al., 2001; Mohapatra et al., 2003). Under steady-state conditions, NF-κB in an inactive form is localised to the cytoplasm by association with the IκB subunit; activation of NF-κB involves the phosphorylation and degradation of IκB NF-κB pathway is activated in primary ATL cells (Mori et al., 1999), a pathway that has received attention as a target for new drugs. Bay11-7082 and DHMEQ, both potent NF-κB inhibitors, strongly induce apoptosis of HTLV-I transfected and ATL cells (Mori et al., 2002; Ohsugi et al., 2005, 2006). Our data show that genistein inhibits p65 translocation into the nucleus and suppresses the expression of c-IAP2, XIAP and survivin. In contrast, although inhibition of p65 translocation and IκBα phosphorylation were not seen after 24 h of genistein treatment, apoptosis was seen at 24 h, suggesting that an NF-κB-dependent pathway is involved in the promotion of apoptosis.

Since genistein has a striking ability to induce accumulation of p53 protein (Yamasaki et al., 2007), it is noteworthy that the majority of HTLV-1-infected cells and also in Hut102 cells, wild-type p53 is present, but in a functionally inactive state. Because strategies to recover p53 activity in ATL cells are now focused on the molecular targets of ATL (Jung et al., 2008), further studies are necessary to elucidate the molecular mechanisms underlying the mode of action of genistein, particularly those related to p53 function and the NF-κB pathway in ATL cells.

Funding

Funding for this project was partially provided by Mishima Kaiun Memorial Foundation 2009.

References

Baxa DM, Luo X, Yoshimura FK (2005) Genistein induces apoptosis in T lymphoma cells via mitochondrial damage. Nutr Cancer 51: 93–101.

Chang KL, Kung ML, Chow NH Su SJ (2004) Genistein arrests hepatoma cells at G2/M phase: involvement of ATM activation and upregulation of p21waf/1cip1 and Wee1. Biochem Pharmacol 67: 717–26.

Hanchard B, Gibbs WN, Lofters W, Campbell M, Williams E, Williams N, Jaffe E, Cranston B, Panchoosingh LD, LaGrenade L, Wilks R, Murphy E, Blattner W, Manns A (1990) HTLV. In: Blattner WA, ed. *Human retrovirology.* New York: Raven Press, pp. 173–83.

Haneji K, Matsuda T, Tomita M, Kawakami H, Ohshiro K, Uchihara JN, Masuda M, Takasu N, Tanaka Y, Ohta T, Mori N (2005) Fucoidan extracted from *Cladosiphon okamuranus* Tokida induces apoptosis of human T-cell leukemia virus type 1-infected T-cell lines and primary adult T-cell leukemia cells. Nutr Cancer 52: 189–201.

Hewitt AL, Singletary KW (2003) Soy extract inhibits mammary adenocarcinoma growth in a syngeneic mouse model. Cancer Lett 192: 133–43.

Jung KJ, Dasgupta A, Huang K, Jeong SJ, Pise-Masison C, Gurova KV, Brady JN (2008) Small-molecule inhibitor which reactivates p53 in human T-cell leukemia virus type 1-transformed cells. J Virol 82: 8537–47.

Karmakar S, Choudhury SR, Banik NL, Ray SK (2009) Combination of N-(4-hydroxyphenyl) retinamide and genistein increased apoptosis in neuroblastoma SK-N-BE2 and SH-SY5Y xenografts. Neuroscience 163: 286–95.

Li W, Frame LT, Hoo KA, Li Y, D'Cunha N, Cobos E (2011) Genistein inhibited proliferation and induced apoptosis in acute lymphoblastic leukemia, lymphoma and multiple myeloma cells in vitro. Leuk Lymphoma 52: 2380–90.

Liao CH, Pan SL, Guh JH, Teng CM (2004) Genistein inversely affects tubulin-binding agent-induced apoptosis in human breast cancer cells. Biochem Pharmacol 67: 2031–8.

Mohan N, Karmakar S, Choudhury SR, Banik NL, Ray SK (2009) Bcl-2 inhibitor HA 14-1 and genistein together adeptly down regulated survival factors and activated cysteine proteases for apoptosis in human malignant neuroblastoma SK-N-BE2 and SH-SY5Y cells. Brain Res 1283: 155–66.

Mohapatra S, Chu B, Wei S, Djeu J, Epling-Burnette PK, Loughran T, Jove R, Pledger WJ (2003) Roscovitine inhibits STAT5 activity and induces apoptosis in the human leukemia virus type 1-transformed cell line MT-2. Cancer Res 63: 8523–30.

Mori N, Yamada Y, Ikeda S, Yamasaki Y, Tsukasaki K, Tanaka Y, Tomonaga M, Yamamoto N, Fujii M (1999) Constitutive activation of NF-kappaB in primary adult T-cell leukemia cells. Blood 93: 2360–8.

Mori N, Yamada Y, Hata T, Ikeda S, Yamasaki Y, Tomonaga M, Yamamoto N (2001) Expression of survivin in HTLV-I-infected T-cell lines and primary ATL cells. Biochem Biophys Res Commun 282: 1110–3.

Mori N, Yamasa Y, Ikeda S, Yamasaki Y, Tsukasaki K, Tanaka Y, Tomonaga M, Yamamoto N, Fujii M (2002) Bay 11-7082 in hibits transcription factor NF-kappaB and induces apoptosis of HTLV-I–infected T-cell lines and primary adult T-cell leukemia cells. Blood 100: 1828–34.

Ohsugi T, Horie R, Kumasaka T, Ishida A, Ishida T, Yamaguchi K, Watanabe T, Umezawa K, Urano T (2005) In vivo antitumor activity of the NF-kappaB inhibitor dehydroxymethylepoxyquinomicin in a mouse model of adult T-cell leukemia. Carcinogenesis 26: 1382–8.

Ohsugi T, Kumasaka T, Ishida A, Ishida T, Horie R, Watanabe T, Umezawa K, Yamaguchi K (2006) In vitro and in vivo antitumor activity of the NF-kappaB inhibitor DHMEQ in the human T-cell leukemia virus type I-infected cell line, HUT-102. Leuk Res 30: 90–7.

Saggioro D, Silic-Benussi M, Biasiotto R, D'Agostino DM, Ciminale V (2009) Control of cell death pathways by HTLV-I proteins. Front Biosci 14: 3338–51.

Su SJ, Chow NH, Kung ML, Hung TC, Chang KL (2003) Effects of soy isoflavones on apoptosis induction and G2-M arrest in human hepatoma cells involvement of caspase-3 activation, Bcl-2 and Bcl-XL downregulation, and Cdc2 kinase activity. Nutr Cancer 45: 113–23.

Taylor JM, Nicot C (2008) HTLV-1 and apoptosis: role in cellular transformation and recent advances in therapeutic approaches. Apoptosis 13: 733–47.

Tomita M, Kawakami H, Uchihara JN, Okudaira T, Masuda M, Takasu N, Matsuda T, Ohta T, Tanaka Y, Ohshiro K, Mori N (2006) Curcumin (diferuloylmethane) inhibits constitutively active NF-kappaB, leading to suppression of cell growth of human T-cell leukemia virus type I-infected T-cell lines and primary adult T-cell leukemia cells. Int J Cancer 118: 765–72.

Tomita M, Kawakami H, Uchihara JN, Okudaira T, Masuda M, Takasu N, Matsuda T, Ohta T, Tanaka Y (2006) Curcumin suppresses constitutive activation of AP-1 by downregulation of Jun D protein in HTLV-1-infected T-cell lines. Leuk Res 30: 313–21.

Yamaguchi K, Kiyokawa T, Futami G, Ishii T, Takatsuki K (1990) HTLV. In: Blattner WA, ed. *Human retrovirology.* New York: Raven Press, pp. 163–71.

Yamasaki M, Fujita S, Ishiyama E, Mukai A, Madhyastha H, Sakakibara Y, Suiko M, Hatakeyama K, Nemoto T, Morishita K, Kataoka H, Tsubouchi H, Nishiyama K (2007) Soy derived isoflavones inhibit the growth of adult T-cell leukemia cells in vitro and in vivo. Cancer Sci 98: 1740–6.

Yu SW, Andrabi SA, Wang H, Kim NS, Poirier GG, Dawson TM, Dawson VL (2006) Apoptosis-inducing factor mediates poly (ADP-ribose) (PAR) polymer-induced cell death. Proc Natl Acad Sci USA 103: 18314–9.

Yu SW, Wang H, Poitras MF, Coombs C, Bowers WJ, Federoff HJ, Poirier GG, Dawson TM, Dawson VL (2002) Mediation of poly (ADP-ribose) polymerase-1-dependent cell death by apoptosis-inducing factor. Science 297: 259–63.

Zhang J, Nagasaki M, Tanaka Y, Morikawa S (2003) Capsaicin inhibits growth of adult T-cell leukemia cells. Leuk Res 27: 275–83.

Received 18 October 2012; accepted 22 February 2013.
Final version published online 18 April 2013.

ANTICANCER RESEARCH *33*: 1893-1898 (2013)

Increased Plasma Caveolin-1 Levels Are Associated with Progression of Prostate Cancer among Japanese Men

SATORU SUGIE[1], SHOICHIRO MUKAI[1], HIROMASA TSUKINO[1], YOSHINOBU TODA[3], TAKENORI YAMAUCHI[2], ICHIRO NISHIKATA[4], YOSHIKI KURODA[2], KAZUHIRO MORISHITA[4] and TOSHIYUKI KAMOTO[1]

Departments of [1]Urology, [2]Public Health, and [4]Tumor and Cellular Biochemistry, Faculty of Medicine, University of Miyazaki, Miyazaki, Japan; [3]Laboratory Medicine, Faculty of Health Care, Tenri Health Care University, Tenri, Japan

Abstract. *Aim: Up-regulation of caveolin-1 (CAV1) is associated with aggressive prostate cancer. Among Caucasian and African-American patients, plasma CAV1 levels are elevated in patients with castration-resistant prostate cancer (CRPC), but not in those with hormone-sensitive prostate cancer (non-CRPC), which implies that CAV1 could be a therapeutic target for CRPC. Here, we evaluated associations between plasma CAV1 levels and these types of cancer in Japanese men, and CAV1 expression in PC3 (CRPC) and LNCaP (non-CRPC) cell lines. Materials and Methods: Plasma samples were obtained from 58 patients with prostate cancer: 36 with CRPC and 22 with non-CRPC. Enzyme-linked immuno sorbent assay (ELISA) kits were used to determine CAV1 plasma levels; qRT-PCR and western blots were used to evaluate the expression of CAV1 mRNA and protein in cell lines. Results: Plasma CAV1 levels in patients with CRPC were greatly higher than in those with non-CRPC (1.46±1.37 ng/ml in CRPC; 0.56±0.32 ng/ml in non-CRPC, $p<0.004$). Western blot and real-time qRT-PCR showed CAV1 protein and mRNA in PC3 cells to be significantly overexpressed compared to its expression in LNCaP cells ($p<0.0001$). Conclusion: Our results showed a relationship between CAV1 expression and prostate cancer progression, and support the possibility of CAV1 as a therapeutic target for CRPC.*

Prostate cancer is the sixth leading cause of cancer-related death among Japanese men (1). In most cases, death from prostate cancer results from metastatic disease. Understanding the mechanisms underlying the progression of prostate cancer will facilitate the development of biomarkers and novel therapeutic strategies to control this devastating malignancy. Caveolin-1, encoded by *CAV1*, is a major structural component of the caveolae, which are specialized plasma membrane invaginations involved in multiple cellular processes such as molecular transport, cell adhesion and signal transduction (2). Although *CAV1* may suppress tumorigenesis under some conditions (3), it is associated with, and contributes to, malignant progression through various mechanisms (4, 5).

The role of *CAV1* in cancer cells remains controversial. It is down-regulated in tumors such as human ovarian carcinoma (6) and head and neck squamous cell carcinoma (SCC) (7), which implies a tumor-suppressor role. However, *CAV1* overexpression is associated with more aggressive behavior, increased recurrence and poorer prognosis in prostate cancer in Caucasian patients (8) and in hepatocellular carcinoma (9). As these discrepancies show, whether *CAV1* up- or down-regulation is an optimistic sign in tumorigenesis, is unclear.

Emerging evidence of a role for *CAV1* in prostate cancer prompted us to investigate its activity in different prostate cancer types, such as castration-resistant prostate cancer (CRPC) and hormone-sensitive prostate cancer. We, therefore, aimed to determine the plasma *CAV1* levels and their association with prostate cancer progression. We also analyzed *CAV1* expression in the PC3 (CRPC model) and LNCaP (non-CRPC model) cell lines. To the best of our knowledge, this is the first study to evaluate the contribution of plasma *CAV1* levels to different types of prostate cancer among Japanese patients.

Materials and Methods

Study participants. The study population consisted of 58 Japanese men with prostate cancer, including 36 with CRPC and 22 with non-CRPC, such as organ-confined tumors. These patients were treated at the Department of Urology, in the Miyazaki Medical University Hospital and its related hospitals between August 2011 and October

Correspondence to: Hiromasa Tsukino, Department of Urology, Faculty of Medicine, University of Miyazaki, 5200 Kihara, Kiyotake-cho, Miyazaki 889-1692, Japan. Tel: +81 985852968, Fax: +81 985856958, e-mail: htsukino@fc.miyazaki-u.ac.jp

Key Words: Caveolin-1, prostate cancer, ELISA, progression.

2012. Tumor grade was evaluated in these samples using the Gleason scoring system. All participants were informed of the details, procedures and objectives of this study. This study was approved by the Ethics Committee of Miyazaki Medical University and related hospitals (Approved number 847, August 2011).

Enzyme-Linked Immuno Sorbent Assay (ELISA) protocols. Blood (5 ml in $EDTA_2Na$) were collected by venipuncture and immediately after blood sampling, plasma was obtained by centrifugation at 12,000 rcf ×g for 15 min at 4°C and stored at –80°C until later analysis. To determine plasma *CAV1* levels, the Human Caveolin-1 ELISA Kit (Uscn Life Science, Inc., Wuhan, China; detection range=0.24-15 ng/ml) was used according to the manufacturer's instructions. To detect the concentration of plasma *CAV1* levels using this ELISA kit, the 60 ng/ml *CAV1* standard was diluted to a concentration range of 0.24-16 ng/ml in duplicate experiments and the absorption was measured

Cell cultures. The androgen-dependent LNCaP and androgen-independent PC3 cancer cell lines (ATCC, Manassas, VA, USA) were grown in Dulbecco's modified Eagle's medium (DMEM; Gibco, Carlsbad, CA, USA) supplemented with 10% fetal bovine serum (FBS; Gibco). Cells were grown in 9.6-cm^2 cell culture dishes at 37°C in a humidified atmosphere of 5% CO_2. Cells were grown to 80% confluence and harvested between passages four and six by trypsinization for analysis. For western blots, cells were seeded in 9.6 cm^2 dishes into 2.5 ml of culture medium for LNCaP cells and PC3 cells respectively. Media were changed every day for five days; cells grown to 90% confluence were passaged by trypsinization. After centrifugation, the cell pellet was resuspended in 1 ml of protease inhibitor, and the cells were counted on a hemocytometer. Aliquots containing 50×10^3 cells in protease inhibitor were frozen at –80°C until used.

Western blot analysis. To analyze protein expression, a western blot method was used. Briefly, samples of protein of 50×10^3 cells were separated on a 12% polyacrylamide gel and the proteins transferred to a polyvinylidene fluoride (PVDF) membrane (transblot transfer medium; BioRad, Hercules, CA, USA). The membrane was probed with rabbit anti-cav1 (Cell Signaling Co., Boston, MA, USA), 1:1,000 diluted in Phosphate Buffered Saline (PBS) with 0.02% (v/v) Tween-20 and 3% (w/v) milk powder. Membranes were incubated with horseradish peroxidase-conjugated goat anti-rabbit immunoglobulins (Dako, Glostrup, Denmark), before detection of antibody binding by chemiluminescence (GE, Tokyo, Japan). Band intensity was measured using a LAS3000 (FUJIFILM, Tokyo, Japan) imaging densitometer and quantified by densitometry using the Image J software (National Institutes of Health, Bethesda, MD, USA).

Real time qRT-PCR. Total RNA was extracted from cells using the RNA Mini kit (Ambion, Paisley, OR, USA) according to the manufacturer's instructions. Genes of interest were amplified from 2 mg DNase I-treated total RNAs using Thunderbird Reverse Transcriptase (ToYoBo, Tokyo, Japan) and random primer. The primers used for real time qRT-PCR were as follows: *CAV1*: forward: 5'-CGCGACCCTAAACACCTCAA-3', reverse: 5'-GCCGTCAAAACTGTGTGTCC-3' (63°C, 40 cycles); and Glyceraldehyde-3-phosphate dehydrogenase (*GAPDH*): forward: 5'-ACCACAGTCCATGCCATCAC-3', reverse: 5'-TCCACCACCC TGTTGCTGTA-3' (63°C, 40 cycles). For real-time qRT-PCR, transcripts were quantified using Applied Biosystems 7300 Real-Time PCR System (Life Technologies, Carlsbad, CA, USA) and Thunderbird SYBR qPCR Mix (ToYoBo, Tokyo, Japan). Experiments were repeated at least three times in triplicate; *GAPDH* was used as an internal control.

Table I. *Clinicopathological features.*

	CRPC	Non-CRPC	*p*-Value*
Age, years mean±SD	68.7±7.7	66.2±5.2	0.18
PSA (ng/ml) mean±SD	41.8±28.4	8.8±4.1	<0.001
Gleason grade n (%)			
Low≤6	2 (5.6)	4 (18.2)	0.045
Intermediate=7	8 (22.2)	9 (40.9)	
High≥8	25 (72.2)	9 (40.9)	
T-grade n (%)			
Low≤T2	7 (19.4)	13 (59.1)	<0.004
High≥T3	29 (80.6)	9 (40.9)	
N n (%)			
Negative	16 (44.4)	22 (100)	<0.001
Positive	20 (55.6)	0 (0)	
M n (%)			
Negative	7 (19.4)	22 (100)	<0.001
Positive	29 (80.6)	0 (0)	
Plasma CAV1 (ng/ml) mean±SD	1.46±1.37	0.56±0.32	<0.004
Total	36	22	

PSA: Prostate-specific antigen; CAV1: caveolin-1; M: metastasis. based on Student's t-test and Pearson's χ^2 test.

Statistical analysis. Statistical analysis was performed using the R i386 2.15.1 software package (Wirtschaftsuniversität Wien, Vienna University of Economics and Business, Vienna, Austria). The significance of differences in plasma *CAV1* levels among CRPC and non-CRPC patients were determined by Student's *t*-tests. $p<0.05$ was considered statistically significant.

Results

Patients' backgrounds and plasma CAV1 levels. Clinicopathological characteristics of patients with CRPC and non-CRPC are summarized in Table I. The mean ages (in years) of patients in the CRPC and non-CRPC groups were 68.3±7.4 (range=61-75) years and 66.9±8.3 (range=59-75) years, respectively. There were no significant differences between the two groups in terms of mean age distribution ($p=0.18$). The mean serum prostate-specific antigen (PSA) levels of the CRPC and non-CRPC groups differed significantly (41.8±28.4 ng/ml and 8.8±4.1 ng/ml, respectively; $p<0.001$). In addition, patients in CRPC and non-CRPC groups differed significantly in clinicopathological characteristics such as Gleason grade, T grade and metastasis (extent, lymph node and bone) (Table I). Mean plasma *CAV1*

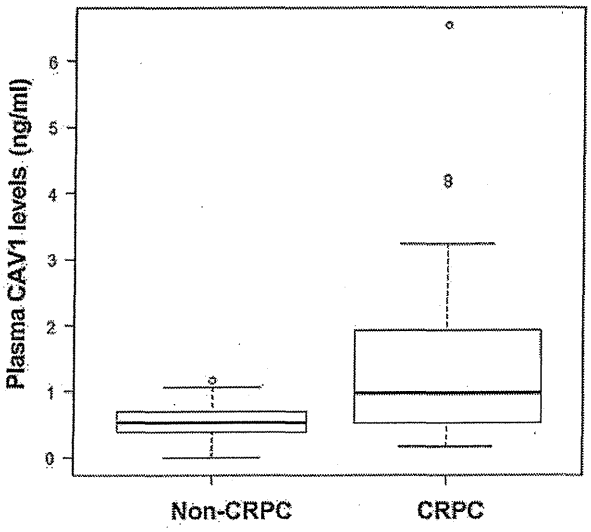

Figure 1. *Plasma Caveolin-1 (CAV1) levels (ng/ml). Plasma CAV1 levels were significantly higher in the CRPC group (1.46±1.37 ng/ml; n=36) than in the non-CRPC group (0.56±0.32 ng/ml; n=22, p<0.004). Boxplot; The boundary of the box closest to zero indicates the 25th percentile, a line within the box marks the median, and the boundary of the box farthest from zero indicates the 75th percentile. Error bars above and below the boxes indicate the 90th and 10th percentiles, respectively.*

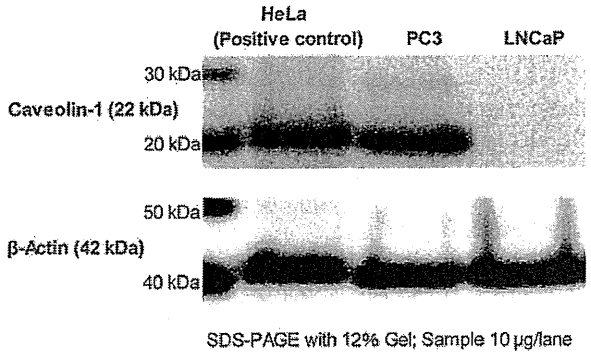

Figure 2. *Western blot analysis showed significantly greater expression of Caveolin-1 (CAV1) in PC3 cells than in LNCaP cells.*

levels in the CRPC group were much higher than in the non-CRPC group (CRPC=1.46±1.37 ng/ml, non-CRPC=0.56±0.32 ng/ml; $p<0.004$; Figure 1).

Western blot analysis. Western blot showed a single immunoreactive band for the CAV1 protein expression at 22 kDa. The loading control, β-Actin at 42 kDa, confirmed that there was equal protein loading (Figure 2). Western blot analysis showed that CAV1 expression was significantly greater in PC3 cells than in LNCaP cells.

Real-time qRT-PCR. Real-time qRT-PCR was performed by prostate cancer cells to examine the *CAV1* mRNA expression, which was found to be significantly greater in PC3 cells than in LNCaP cells (*CAV1/GAPDH*, PC3 *vs.* LNCaP=1 *vs.* 0.002; $p<0.001$).

Discussion

This study investigated whether *CAV1* expression varied between Japanese patients with CRPC and in patients with androgen-sensitive prostate cancer. We also investigated differences in CAV1 protein and mRNA expression between PC3 cells (CRPC model) and LNCaP cells (non-CRPC model). Our data showed increasing levels of plasma *CAV1* to have prognostic potential for prostate cancer progression.

CAV1 has been linked with various types of cancers over the past decade, during which it was most extensively studied in breast and prostate cancer. It was found that *CAV1* levels in tumor tissue and in plasma may be associated with tumor protection or progression (10). In prostate cancer, in particular, elevated *CAV1* expression was observed in tumor tissues in humans and in a mouse model, compared to non-tumor tissues (11-13). Another study implied that *CAV1* and cancer-promoting growth factors collaborate in prostate cancer progression, although more evidence is needed (14). CAV1 is thought to suppress tumor growth and metastasis in human breast and colon cancer (15, 16). However, CAV1 function may differ among different organs, and CAV1 could thus exert opposing effects, resulting in promotion or suppression of tumor progression. For example, CAV1 expression increased in tumor samples from the kidney, prostate and stomach, and re-expression has been found in some advanced adenocarcinomas (17). Elevated CAV1 expression is associated with progression of some adenocarcinomas, such as prostate carcinoma (18), and in adult T-cell leukemia (19). Interestingly, activated CAV1 expression is associated with higher grades of prostate cancer, although few significant relationships have been identified between CAV1 expression and tumor multiplicity, recurrence, progression, or overall survival (16).

Li et al. showed that CAV1 was secreted by mouse and human prostate cancer cell lines, and that secreted CAV1 promoted cancer cell survival and clonal growth *in vitro* (20, 21). They further showed that tumor cell-secreted CAV1 promoted pro-angiogenic activities in prostate cancer through the phosphoinositol-3-kinase (PI3K)–protein kinase B (AKT)–endothelial nitric oxide synthase (eNOS) signaling pathway (22). Regarding the mechanisms through which CAV1 mediates oncogenic activities, they showed CAV1 to hold AKT in an activated form in prostate cancer cells by

binding to and inhibiting the serine/threonine protein phosphatases PP1 and PP2A (14). Thus, engagement of CAV1 as a tumor metastasis promoter depends on the cellular context, and at the molecular level, by the signaling molecules and signaling pathways affected and regulated by CAV1. We hypothesize that altered CAV1 expression interferes with homeostasis, and increases the frequency of prostate cancer.

Our results also show that *CAV1* is associated with tumor progression and metastasis, and is distinctly elevated in androgen-resistant tumors. Therefore, *CAV1* could be a marker for an aggressive form of cancer (18, 22, 23-27).

Suppression of CAV1 expression has been shown to restore sensitivity to androgens in androgen-insensitive tumors (13). Our findings, together with data from other studies, suggest that CAV1 is involved in disease pathogenesis and progression. Further study of its role in prostate cancer can contribute to the understanding of this disease, and possibly offer novel targeted therapeutic approaches. Although associations between *CAV1* and high-risk tumors were identified in this study, we still cannot confirm *CAV1* to be a marker for high-risk aggressive tumors, even at the phase when tumors are localized in the prostate and thus are still curable. To do so would require monitoring *CAV1* levels in a follow-up study over the course of prostate cancer progression from its initial stages. Our results should also be verified in a larger group of patients, including those with disseminated disease.

Conflicts of Interest

The Authors have no potential conflicts of interest.

References

1 Committee for Establishment of the Guidelines on Screening for Prostate Cancer. Japanese Urological Association: Updated Japanese Urological Association Guidelines on prostate-specific antigen-based screening for prostate cancer in 2010. Int J Urol *17(10)*: 830-838, 2010.

2 Shaul PW and Anderson RG: Role of plasmalemmal caveolae in signal transduction. Am J Physiol *275*: L843-L851, 1998.

3 Williams TM and Lisanti MP: Caveolin-1 in oncogenic transformation, cancer, and metastasis. Am J Physiol *288*: C494-C506, 2005.

4 Cavallo-Medved D, Mai J, Dosescu J, Sameni M and Sloane BF: Caveolin-1 mediates the expression and localization of cathepsin B, pro-urokinase plasminogen activator and their cell-surface receptors in human colorectal carcinoma cells. J Cell Sci *118*: 1493-1503, 2005.

5 Woodman SE, Ashton AW, Schubert W, Lee H, Williams TM, Medina FA, Wyckoff JB, Combs TP and Lisanti MP: Caveolin-1 knockout mice show an impaired angiogenic response to exogenous stimuli. Am J Pathol *162*: 2059-2068, 2003.

6 Wiechen K, Diatchenko L, Agoulnik A, Scharff KM, Schober H, Arlt K, Zhumabayeva B, Siebert PD, Dietel M, Schafer R and Sers C: Caveolin-1 is down-regulated in human ovarian carcinoma and acts as a candidate tumor suppressor gene. Am J Pathol *159*: 1635-1643, 2001.

7 Zhang H, Su L, Muller S, Tighiouart M, Xu Z, Zhang X, Shin HJ, Hunt J, Sun SY, Shin DM and Chen ZG: Restoration of caveolin-1 expression suppresses growth and metastasis of head and neck squamous cell carcinoma. Br J Cancer *99*: 1684-1694, 2008.

8 Karam JA, Lotan Y, Roehrborn CG, Ashfaq R, Karakiewicz PI and Shariat SF: Caveolin-1 overexpression is associated with aggressive prostate cancer recurrence. Prostate *67*: 614-622, 2007.

9 Zhang ZB, Cai L, Zheng SG, Xiong Y and Dong JH: Overexpression of caveolin-1 in hepatocellular carcinoma with metastasis and worse prognosis: correlation with vascular endothelial growth factor, microvessel density and unpaired artery. Pathol Oncol Res *15*: 495-502, 2009.

10 Williams TM and Lisanti MP: Caveolin-1 in oncogenic transformation, cancer, and metastasis. Am J Physiol Cell Physiol *288*: C494-C506, 2005.

11 Tahir SA, Ren CZ, Timme TL, Gdor Y, Hoogeveen R, Morrisett JD, Frolov A, Ayala G, Wheeler TM and Thompson TC: Development of an immunoassay for serum caveolin-1: A novel biomarker for prostate cancer. Clin Cancer Res *9*: 3653-3659, 2003.

12 Nasu Y, Timme TL, Yang G, Bangma CH, Li L, Ren C, Park SH, DeLeon M, Wang J and Thompson TC: Suppression of caveolin expression induces androgen sensitivity in metastatic androgen-insensitive mouse prostate cancer cells. Nat Med *4*: 1062-1064, 1998.

13 Yang G, Truong LD, Wheeler TM and Thompson TC: Caveolin-1 expression in clinically confined human prostate cancer: A novel prognostic marker. Cancer Res 59: 5719-5723, 1999.

14 Li L, Ren C, Yang G, Goltsov AA, Tabata K and Thompson TC: Caveolin-1 promotes autoregulatory, Akt-mediated induction of cancer-promoting growth factors in prostate cancer cells. Mol Cancer Res *7*: 1781-1791, 2009.

15 Lee SW, Reimer CL, Oh P, Campbell DB and Schnitzer JE: Tumor cell growth inhibition by caveolin re-expression in human breast cancer cells. Oncogene *16*: 1391-1397, 1998.

16 Rajjayabun PH, Garg S, Durkan GC, Charlton R, Robinson MC and Mellon JK: Caveolin-1 expression is associated with high-grade bladder cancer. Urology *58*: 811-814, 2001.

17 Wiechen K, Sers C, Agoulnik A, Arlt K, Dietel M, Schlag PM and Schneider U: Down-regulation of caveolin-1, a candidate tumor suppressor gene, in sarcomas. Am J Pathol *158*: 833-839, 2001.

18 Thompson TC, Tahir SA, Li L, Watanabe M, Naruishi K, Yang G, Kadmon D, Logothetis CJ, Troncoso P, Ren C, Goltsov A and Park S: The role of caveolin-1 in prostate cancer: clinical implications. Prostate Cancer Prostatic Dis *13(1)*: 6-11, 2010.

19 Sawada S, Ishikawa C, Tanji H, Nakachi S, Senba M, Okudaira T, Uchihara JN, Taira N, Ohshiro K, Yamada Y, Tanaka Y, Uezato H, Ohshima K, Sasai K, Burgering BM, Duc Dodon M, Fujii M, Sunakawa H and Mori N: Overexpression of caveolin-1 in adult T-cell leukemia. Blood *115*: 2220-2230, 2010.

20 Li L, Ren CH, Tahir SA, Ren C and Thompson TC: Caveolin-1 maintains activated AKT in prostate cancer cells through scaffolding domain binding site interactions with and inhibition of serine/threonine protein phosphatases PP1 and PP2A. Mol Cell Biol *23*: 9389-9404, 2003.

21 Li L, Yang G, Ebara S, Satoh T, Nasu Y, Timme TL, Ren C, Wang J, Tahir SA and Thompson TC: Caveolin-1 mediates testosterone-stimulated survival/clonal growth and promotes metastatic activities in prostate cancer cells. Cancer Res *61*: 4386-92, 2001.

22 Tahir SA, Yang G, Ebara S, Timme TL, Satoh T, Li L, Goltsov A, Ittmann M, Morrisett JD and Thompson TC: Secreted caveolin-1 stimulates cell survival/clonal growth and contributes to metastasis in androgen-insensitive prostate cancer. Cancer Res *61*: 3882-3885, 2001.

23 Watanabe M, Yang G, Cao GW, Tahir SA, Naruishi K, Tabata K, Fattah EA, Rajagopalan K, Timme TL, Park S, Kurosaka S, Edamura K, Tanimoto R, Demayo FJ, Goltsov AA and Thompson TC: Functional analysis of secreted caveolin-1 in mouse models of prostate cancer progression. Mol Cancer Res *7*: 1446-1455, 2009.

24 Tahir SA, Yang G, Ebara S, Timme TL, Satoh T, Li L, Goltsov A, Ittmann M, Morrisett JD and Thompson TC: Secreted caveolin-1 stimulates cell survival/clonal growth and contributes to metastasis in androgen-insensitive prostate cancer. Cancer Res *61*: 3882-3885, 2001.

25 Yang G, Truong LD, Timme TL, Ren C, Wheeler TM, Park SH, Nasu Y, Bangma CH, Kattan MW, Scardino PT and Thompson TC: Elevated expression of caveolin is associated with prostate and breast cancer. Clin Cancer Res *4*: 1873-1880, 1998.

26 Thompson TC, Timme TL, Li L and Goltsov A: Caveolin-1, a metastasis-related gene that promotes cell survival in prostate cancer. Apoptosis *4*: 233-237, 1999.

27 Mouraviev V, Li LK, Tahir SA, Yang G, Timme TM, Goltsov A, Ren C, Satoh T, Wheeler TM, Ittmann MM, Miles BJ, Amato RJ, Kadmon D and Thompson TC: The role of caveolin-1 in androgen insensitive prostate cancer. J Urol *168*: 1589-1596, 2002.

Received February 28, 2013
Revised March 28, 2013
Accepted March 29, 2013

OPEN

Citation: Blood Cancer Journal (2013) 3, e132; doi:10.1038/bcj.2013.30

www.nature.com/bcj

ORIGINAL ARTICLE

Oral administration of an HSP90 inhibitor, 17-DMAG, intervenes tumor-cell infiltration into multiple organs and improves survival period for ATL model mice

E Ikebe[1], A Kawaguchi[2,3,13], K Tezuka[4,13], S Taguchi[1,13], S Hirose[1], T Matsumoto[1], T Mitsui[1], K Senba[1], A Nishizono[1], M Hori[5], H Hasegawa[6], Y Yamada[6], T Ueno[4], Y Tanaka[7], H Sawa[3], W Hall[8], Y Minami[9], KT Jeang[10], M Ogata[11], K Morishita[12], H Hasegawa[2], J Fujisawa[4] and H Iha[1]

In the peripheral blood leukocytes (PBLs) from the carriers of the human T-lymphotropic virus type-1 (HTLV-1) or the patients with adult T-cell leukemia (ATL), nuclear factor kappaB (NF-κB)-mediated antiapoptotic signals are constitutively activated primarily by the HTLV-1-encoded oncoprotein Tax. Tax interacts with the I κB kinase regulatory subunit NEMO (NF-κB essential modulator) to activate NF-κB, and this interaction is maintained in part by a molecular chaperone, heat-shock protein 90 (HSP90), and its co-chaperone cell division cycle 37 (CDC37). The antibiotic geldanamycin (GA) inhibits HSP90's ATP binding for its proper interaction with client proteins. Administration of a novel water-soluble and less toxic GA derivative, 17-dimethylaminoethylamino-17-demethoxygeldanamycin hydrochloride (17-DMAG), to Tax-expressing ATL-transformed cell lines, C8166 and MT4, induced significant degradation of Tax. 17-DMAG also facilitated growth arrest and cellular apoptosis to C8166 and MT4 and other ATL cell lines, although this treatment has no apparent effects on normal PBLs. 17-DMAG also downregulated Tax-mediated intracellular signals including the activation of NF-κB, activator protein 1 or HTLV-1 long terminal repeat in Tax-transfected HEK293 cells. Oral administration of 17-DMAG to ATL model mice xenografted with lymphomatous transgenic Lck-Tax (Lck proximal promoter-driven Tax transgene) cells or HTLV-1-producing tumor cells dramatically attenuated aggressive infiltration into multiple organs, inhibited *de novo* viral production and improved survival period. These observations identified 17-DMAG as a promising candidate for the prevention of ATL progression.

Blood Cancer Journal (2013) **3**, e132; doi:10.1038/bcj.2013.30; published online 16 August 2013

Keywords: 17-DMAG; molecular chaperon; Tax; ATL; apoptosis; transgenic model

INTRODUCTION

Nuclear factor kappaB (NF-κB) is a transcription factor that regulates immune and antiapoptotic responses to multiple extracellular stresses.[1,2] Under normal conditions, most NF-κB molecules are sequestered in the cytoplasm by the inhibitor I κB. In response to cellular stress, I κB is rapidly phosphorylated by the NF-κB activator I κB kinase (IKK) and ubiquitylated for degradation by the proteasome. This frees NF-κB for translocation into the nucleus, where it directs the transcriptional activation of NF-κB-responsive genes.[3,4] IKK is comprised of three different subunits, IKKα, IKKβ and IKKγ/NEMO (NF-κB essential modulator). IKKγ is also known as NF-κB essential modulator (NEMO). NEMO trimerizes rapidly in response to extracellular stimuli, such as the pro-inflammatory cytokine tumor necrosis factor-α (TNF-α), and recruits the two catalytic subunits, IKKα/β, to form a highly phosphorylated active IKK holoenzyme.[5] Several genetic studies have shown that cytokine-triggered activation of what is termed the canonical NF-κB activation pathway is primarily dependent on NEMO and IKKβ,[6,7] whereas IKKα activity is required for the development of the skin, limbs and lymph nodes.[8,9] Upon stimulation, several accessory proteins are recruited to IKK, and the molecular size of this active IKK complex reaches more than 1 MDa.[10,11] The molecular chaperone heat-shock protein 90 (HSP90) and its co-chaperone cell division cycle 37 (CDC37) are components of this high molecular weight (HMW)-IKK complex, and they play crucial roles in maintaining the activity of the complex.[12] The antibiotic geldanamycin (GA) specifically binds to the ATPase domain of HSP90 and inhibits its function as a molecular chaperone, resulting in the efficient inhibition of TNF-α-mediated activation of NF-κB.[12,13]

The human T-lymphotropic virus type-1 (HTLV-1), which is the etiologic agent of adult T-cell leukemia (ATL), encodes the oncoprotein Tax.[14–16] Tax activates NF-κB by interacting

[1]Department of Infectious Diseases, Faculty of Medicine, Oita University, Yufu, Japan; [2]Department of Pathology, National Institute of Infectious Diseases, Musashimurayama, Japan; [3]Department of Molecular Pathobiology, 21st Century COE Program for Zoonosis Control, Hokkaido University Research Center for Zoonosis Control, Sapporo, Japan; [4]Department of Microbiology, Kansai Medical University, Moriguchi, Japan; [5]Department of Hematology, Ibaraki Prefectural Central Hospital, Kasama, Ibaraki, Japan; [6]Department of Laboratory Medicine, Nagasaki University Graduate School of Biomedical Sciences, Nagasaki, Japan; [7]Department of Immunology, Graduate School of Medicine, University of the Ryukyus, Nishihara, Japan; [8]Department of Medical Microbiology, Centre for Research in Infectious Diseases, Conway Institute of Biomolecular and Biomedical Research, University College Dublin, Dublin, Ireland; [9]Department of Biotechnology, Maebashi Institute of Technology, Maebashi, Japan; [10]Molecular Virology Section, Laboratory of Molecular Microbiology, National Institute of Allergy and Infectious Diseases, Bethesda, MD, USA; [11]Department of Hematology, Faculty of Medicine, Oita University, Yufu, Japan and [12]Division of Tumor and Cellular Biochemistry, Department of Medical Sciences, Faculty of Medicine, University of Miyazaki, Miyazaki, Japan. Correspondence: Dr H Iha, Department of Infectious Diseases, Faculty of Medicine, Oita University, 1-1 Idaigaoka, Hasama, Yufu, Oita 879-5593, Japan.
E-mail: hiha@oita-u.ac.jp
[13]These authors contributed equally to this work.
Received 25 June 2012; revised 24 June 2013; accepted 28 June 2013

physically with NEMO.[10,17] NF-κB activation mediated by this Tax–NEMO interaction is similar to that of the TNF-α-triggered 'canonical' pathway. Tax induces IKK phosphorylation, ubiquitylation and proteasome-dependent degradation of I κB, thereby inducing the translocation of NF-κB into the nucleus.[18,19] However, in contrast to the TNF-α-triggered canonical pathway, which is transient and mostly IKKβ dependent, Tax-mediated NF-κB activation is persistent and utilizes both the IKKα and IKKβ subunits.[20,21] From these observations, we speculated that oncogenic Tax-mediated activation of NF-κB is distinguishable from the canonical NF-κB activation pathway, and indeed, we have succeeded in inhibiting Tax-mediated NF-κB activation using selected sets of NEMO-mutant peptides.[11]

Those earlier studies led us to ask whether GA can inhibit Tax-mediated HMW-IKK formation and suppress NF-κB activation as has been demonstrated in the TNF-α-triggered canonical pathway. To address this, we treated ATL cell lines or HEK293 cells transfected with a Tax expression vector with GA or its less toxic derivative 17-dimethylaminoethylamino-17-demethoxygeldanamycin hydrochloride (17-DMAG).[22] We found that these HSP90 inhibitors downregulated Tax-mediated intracellular activity including the activation of NF-κB, activator protein 1 and HTLV-1 long terminal repeat (HTLV-1-LTR). These findings prompted us to investigate the molecular mechanisms by which HSP90 inhibitors disrupt Tax-mediated signaling in ATL cells. We found that the stability of Tax in ATL cells is heavily dependent on the HSP90/CDC37 chaperones and that Tax is rapidly degraded without these chaperones following the addition of HSP90 inhibitors. Apoptosis of ATL cells was also induced by GA and 17-DMAG. Finally, the oral administration of 17-DMAG to severe combined immunodeficient (SCID) mice transplanted with lymphomatous cells bearing Lck proximal promoter-driven Tax transgene (Lck-Tax) cells[23] markedly inhibited the aggressive infiltration of these Lck-Tax cells into multiple organs. The same procedure to the humanized NOG (huNOG) mice inoculated with HTLV-1-producing Jurkat cells also resulted in the suppression of *de novo* viral production and improved the survival period.

MATERIALS AND METHODS

Ethics statement

This study was carried out in strict accordance with the recommendations in the Guidelines for Proper Conduct of Animal Experiments, Science Council of Japan (http://www.scj.go.jp/en/animal/index.html). All procedures involving animals and their care were approved by the Animal Care Committee of Oita University, National Institute of Infectious Diseases and Kansai Medical University in accordance with the Regulations for Animal Experiments in Oita University (approval ID: 24-22).

Chemicals, cells and cell culture conditions

All chemicals used in this study including 17-DMAG[22] and cell lines or peripheral blood leukocytes (PBLs) were described in Supplementary Information.

Coimmunoprecipitation and immunoblot

One million cells of MT4 and C8166 treated with or without 17-DMAG and HEK293 cells transfected with each plasmid (maximum 1 μg) by FugeneHD (Roche Applied Science, Tokyo, Japan) for 40 h were lysed with coimmunoprecipitation (Co-IP) buffer. Each 200 μg of precleared (with 30 μl of protein G agarose, CalBiochem, Millipore Corporation, Billerica, MA, USA) lysates was incubated with 2 μg of rabbit polyclonal anti-HSP90 (Stressgen Bioreagents, Ann Arbor, MI, USA) or rabbit anti-FLAG antibody (Sigma-Aldrich, St Louis, MO, USA) for at least 3 h at 4° C. Antibody–protein G complexes were washed, resolved by sodium dodecyl sulfate-polyacrylamide gel electrophoresis and transferred onto a polyvinylidene difluoride membrane, and specific proteins were detected by monoclonal anti-Tax, -HSP90 (Stressgen), -Flag, -tubulin (Sigma) or polyclonal anti-IKKb (Cell Signaling Technology) antibodies, respectively.

Real-time quantitative reverse transcriptase-PCR by the LightCycler system

Total RNA from MT4 cells treated with or without 17-DMAG was isolated using ISOGEN (Wako Pure Chemical Industries, Ltd., Osaka, Japan), and contaminated DNA was removed. cDNA was constructed by the Thermoscript reverse transcriptase-PCR system (Invitrogen, Life Technologies Japan Co., Tokyo, Japan), and real-time quantitative PCRs for Tax and glucose-6-phosphate 1-dehydrogenase were performed on a Roche LC480 system (Roche) with indicated probe and primer sets.

Cell viability assay

Cell lines or PBLs from ATL patients or healthy donors were treated with 2.5 μM of 17-DMAG for 1–4 days. After every 24 h incubation, cell viabilities were counted with Cell Counting Kit (Dojindo Laboratories, Kumamoto, Japan).

Caspase-3/7 assay

Cells used in the 'cell viability assay' were also subjected for apoptosis activity with cappase-3/7 assay and GLOMAX 96 microplate luminometer (Promega KK, Tokyo, Japan).

Plasmids

The details of plasmid pSG5-Tax,[24] HSP90,[25] Cdc37,[26] CMV-Tax or LTR-Tax[11] and CoralHue-Tax or −CDC37 vectors (MBL Co. Ltd., Nagoya, Japan)[27] are described in Supplementary Information.

Luciferase assay

HEK293 cells were transfected with plasmid DNA mixture containing the reporter plasmids (NF-κB-Luc or HTLV-1-LTR-Luc[11] and RSV-β-galactosidase as a transfection indicator) and Tax expression vectors (pSG5-Tax, CMV-Tax or LTR-Tax) by FugeneHD. After 24 h incubation of the transfection, where indicated, 17-DMAG at concentrations listed in the figures was added, and cells were further incubated for 16 h. Cell lysates were subjected to the luciferase assay kit and GLOMAX 96.

Microscopic observation of cells

HEK293 cells were transfected with phmKGN-MC-Tax and phmKGC-MN-Cdc37 or its mutant −Cdc37(N200) or −Cdc37(N180) for 48 h and then treated with 1 μM of Hoechst 34442 (Sigma). Light and fluorescent (green fluorescent protein (GFP) or Hoechst 34442) microscopic observation and photography were performed by BZ-9000 Biorevo (Keyence Co. Ltd., Osaka, Japan).

Transfer of Lck-Tax transgenic cells to SCID mice and treatment with 17-DMAG

SCID mice were injected intraperitoneally with 2×10^6 Lck-Tax cells.[23] 17-DMAG was administered orally 5 days per week, with 5, 15 or 30 mg/kg for 2–3 weeks, and then mice were sacrificed for pathological examination.

HTLV-1 infection to huNOG and flow cytometric analysis of peripheral bloods

Suspension of irradiated 1×10^6 HTLV-1-producing JEX cells was inoculated intraperitoneally into huNOG mice[28] at the age between 24 and 28 weeks. Peripheral blood cells were routinely collected every 2 weeks after infection. Spleen, bone marrow and lymph node were collected, and PBLs were stained with florescent dye-conjugated antibodies against human cellular surface markers.

DNA isolation and quantification of proviral load

Genomic DNA was extracted from single cell suspension of tissue or peripheral blood followed by the conventional phenol extraction method. Proviral load was measured by quantitative PCR as previously described.[29]

Histopathological examination and immunohistochemistry

Tissues were directly fixed in the neutral buffered formalin (Sigma), embedded in paraffin, sectioned and stained with hematoxylin and eosin. Peripheral blood smears were prepared using Giemsa staining and examined by light microscopy.

For details, see Supplementary Information.

RESULTS

The NF-κB-activating Tax–HSP90–IKK ternary complex is disaggregated by HSP90 inhibitors that induce Tax degradation

The molecular chaperone HSP90 and its co-chaperone CDC37 are both recruited to IKK and play essential roles in TNF-α-triggered HMW-IKK formation and subsequent NF-κB activation. The addition of the HSP90-specific inhibitor GA completely suppresses NF-κB signaling.[12] As we previously demonstrated that the expression of Tax also resulted in the formation of a HMW-IKK complex for activating NF-κB,[11] we speculated that the inhibition of HSP90 function by GA would also affect Tax-mediated NF-κB signaling. First, using Tax-expressing MT4 cells, we confirmed the interaction of Tax with HSP90 in the same protein complex by Co-IP assays (Figure 1a). We then treated MT4 cells for 24 h with a newly developed, less toxic and water-soluble GA derivative, 17-DMAG,[22] to evaluate its effects on the formation of a Tax-induced ternary complex, Tax–HSP90–IKK. To our surprise, the amount of Tax in MT4 cells decreased progressively with increasing doses of 17-DMAG (Figure 1b, upper panel) despite no apparent changes in the amount of HSP90 in the same lysate (data not shown). Under these conditions, the interaction between HSP90 and IKKβ was clearly reduced with increasing doses of 17-DMAG (Figure 1b, middle panel), whereas the amount of HSP90 immunoprecipitated throughout this range of concentrations was unchanged (Figure 1b, lower panel).

We then examined the kinetics of Tax degradation in MT4 cells treated with 17-DMAG. Reductions in Tax levels were observed in cells treated for 12 h and continued over time until by 48 h, when the level of Tax became undetectable (Figure 1c). This 17-DMAG-induced Tax degradation stabilized I κBα, whereas another NF-κB inhibitor dexamethasone had no effects (Supplementary Figure 1). Tax degradation by 17-DMAG occurred prior to mRNA suppression as the marked decrease of Tax mRNA was not observed until 24 h after treatment (Figure 1d), whereas protein level of Tax was obviously decreased by 12 h (compare Figures 1c and d). Our previous study indicated that Tax degradation is partly induced by caspase,[30] and polyubiquitylation had little effects on its cellular stability.[31] We therefore re-evaluated which pathway is responsible for the 17-DMAG-induced Tax degradation (Figure 1e). Tax degradation was partly blocked by the caspase inhibitor zVAD-fmk[30] and by autophagy inhibitors 3-methyladenine (3-MA) and 5-aminoimidazole-4-carboxamide-1-b-D-ribofuranoside (AICAR)[32] but not by the proteasome inhibitor MG132. Similar findings were obtained from parallel studies using another ATL cell line, C8166 (data not shown), although more investigation is needed for fully understanding of Tax instability.

GA and its derivatives are known to suppress a variety of intracellular signaling pathways, including NF-κB activation by inhibiting IKK.[12,33] One of the most important functions of NF-κB is to protect cells from apoptotic stress. A portion of 2.5 μM of 17-DMAG is sufficient to induce Tax degradation (Figure 1c) and I κBα stabilization (Supplementary Figure 1), which implies the suppression of ATL cell growth; however, it is important to know whether this concentration is toxic to normal PBLs. We, therefore, confirmed the median inhibitory concentrations of 17-DMAG for several ATL or non-ATL cell lines along with normal PBLs.

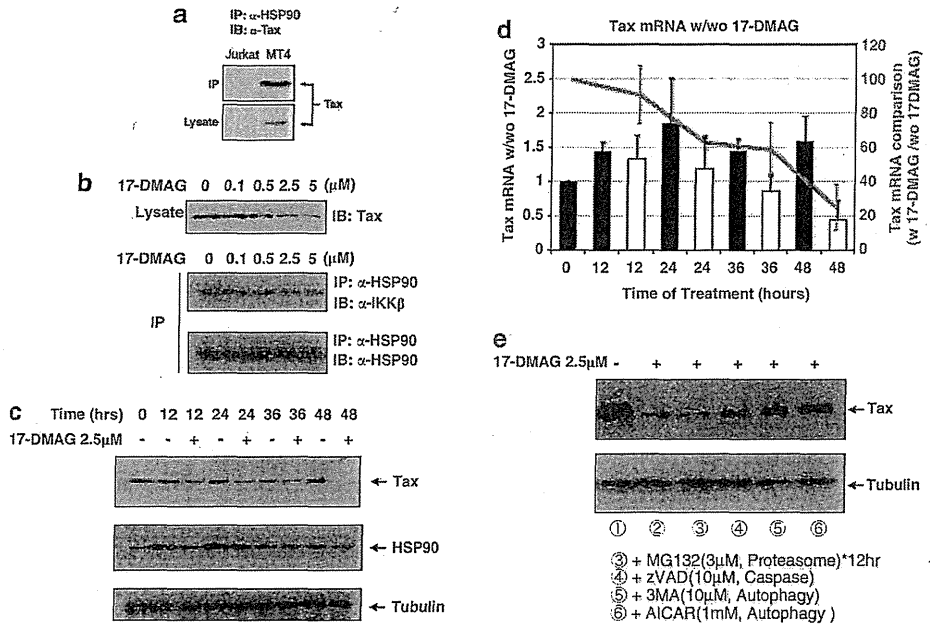

Figure 1. 17-DMAG inhibits HSP90–Tax–IKK ternary complex formation and induces Tax degradation in ATL cells. (**a**) Co-IP of Tax and HSP90. *Four million Jurkat or MT4 cells were lysed with Co-IP buffer, and 50 μg total of cell lysates were subjected to IP with 2 μg of rabbit polyclonal* anti-HSP90 antibody, followed by immunoblot (IB) with mouse monoclonal anti-Tax antibody (upper panel). The amount of expressed Tax in each cell line was verified by IB with anti-Tax against 10 μg of cell lysates (lower panel). (**b**) 17-DMAG's effects on Tax expression level and *physical interaction between HSP90 and IKKβ in MT4 cells. Four million MT4 cells were treated with the indicated concentrations of 17-DMAG* for 16 h. Co-IP and IB against immunoprecipitates or lysates were carried out as in panel **a**. (**c**) Ten micrograms of each cell lysate from MT4 cells treated with or without 2.5 μM of 17-DMAG for the indicated periods were subjected to sodium dodecyl sulfate-polyacrylamide gel electrophoresis, and Tax (upper panel), HSP90 (middle panel) or tubulin (lower panel) expression was detected using monoclonal anti-Tax, anti-HSP90 or anti-tubulin antibodies. (**d**) Expression levels of Tax in 17-DMAG-treated MT4 cells. mRNAs were prepared from the same aliquots of MT4 cells described in panel **c**. mRNAs from 17-DMAG-untreated fractions (black bars) and 17-DMAG-treated fractions (2.5 μM, white bars) with indicated time courses were analyzed with the universal probes (Roche) and primers through the LightCycler PCR method according to the manufacturer's direction. Comparison of Tax mRNAs with or without 17-DMAG was also indicated with a red line graph as a division of Tax mRNA with 17-DMAG/without 17-DMAG at each time point. (**e**) Four million MT4 cells were treated with 2.5 μM 17-DMAG for 24 h (lanes 2–6) and then additional 3 μM MG132 for 12 h (lane 3), 10 μM zVAD-fmk (lane 4) and 3-MA (lane 5) and 1 mM AICAR (lane 6) for 24 h. Lysates were prepared for IB of Tax and tubulin.

The median inhibitory concentrations to ATL cells vary from 0.06 to 2.33 μM, which is much lower than that of non-ATL Jurkat cells (9.32 μM), and three PBLs did not show any significant growth suppression with 10 μM of 17-DMAG (Supplementary Figure 2). We set the concentration of 17-DMAG at 2.5 μM and measured the effects on the viability of ATL cells (cell lines established from ATL patients' PBLs or cord blood cocultured with ATL patients' PBLs or primary PBLs of ATL patients) and other leukemic cells, as well as PBLs from HTLV-1-negative controls. Most of the ATL cell lines treated with 17-DMAG exhibited a rapid decrease in viability, whereas normal PBLs were unaffected by the drug (Figure 2a). 17-DMAG treatment also resulted in a marked increase in caspase-3/7 activity in most of the ATL cell lines while having no significant caspase perturbation in control PBLs (Figure 2b).

Downregulation of Tax occurs at the post-transcriptional stage

We then proceeded to examine the details of 17-DMAG-dependent inhibitory effects on the Tax–HSP90–IKK ternary complex by transfection of two different Tax expression vectors into HEK293 cells. One was driven by the simian virus 40 early promoter and

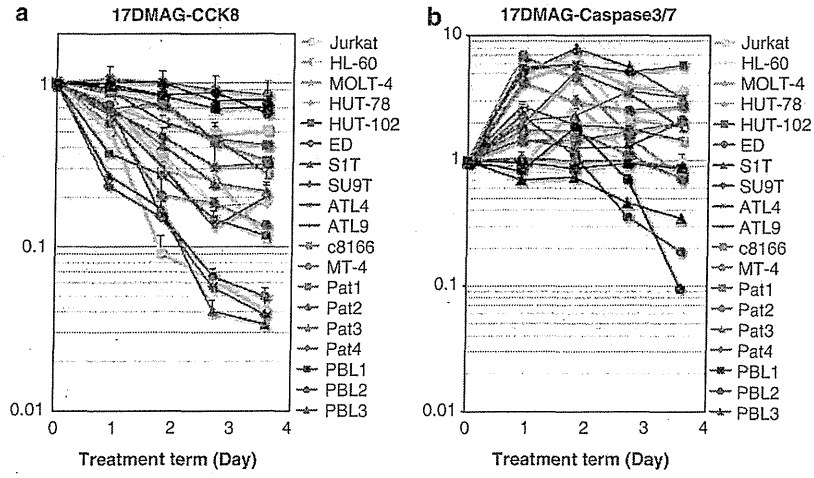

Figure 2. 17-DMAG induces growth arrest and apoptosis in ATL cells. Two million cells from each ATL cell line established from ATL patients' PBLs (HUT-102, ED, S1T, SU9T, ATL4 and ATL9; red lines), ATL cell lines established by coculture of cord blood and ATL patients' PBLs (C8166 and MT4; orange lines), PBLs from ATL patients (Pat1 to Pat4; purple lines), non-ATL leukemic cell lines (Jurkat, HL-60, MOLT-4 and HUT-78; yellow lines) or healthy donors (PBL1, PBL2 and PBL3; blue lines) were treated with 2.5 μM of 17-DMAG for 1–4 days. After each 24 h incubation, 10^4 (**a**) or 5×10^3 (**b**) cells were transferred to each well of a 96-well plate. (**a**) One-tenth volume of Cell Counting Kit 8 solution (Dojindo) was added to each fraction. Thirty minutes after incubation, the absorbance at 465 nm was measured using an E-max precision microplate reader (Molecular Devices Japan Co. Ltd., Tokyo, Japan). (**b**) The same volume of Apo-ONE homogeneous Caspase-3/7 assay solution was added to cells, and chemical luminescence was quantified with GloMax luminometer (Promega).

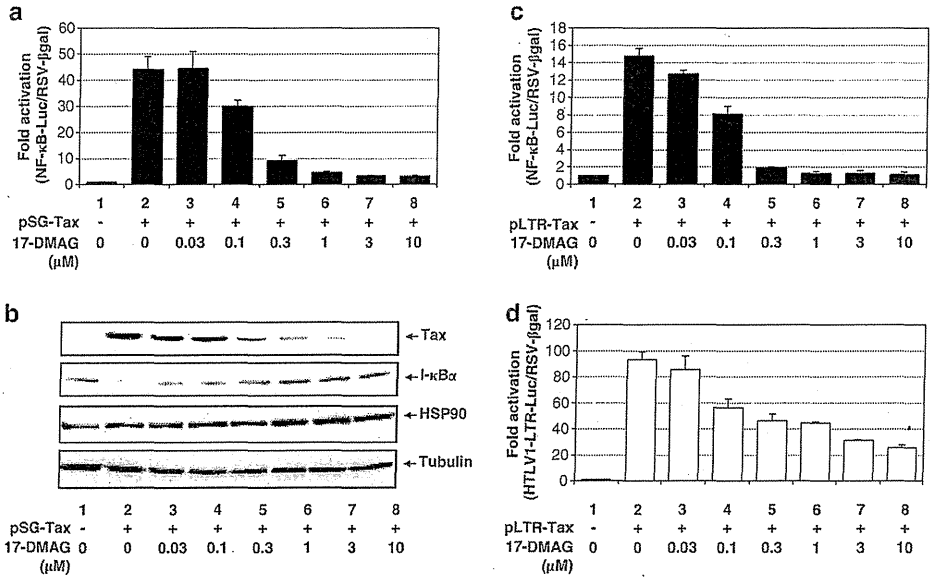

Figure 3. 17-DMAG downregulates all the Tax-mediated signaling in HEK293 cells. Fifty thousand HEK293 cells in each well on a 12-well plate were transfected with 0.5 μg of pSG-Tax (**a**, **c**) or pLTR-Tax along with 50 ng of NF-κB-luciferase (**a**, **c**) or HTLV-1-LTR-luciferase (**d**) and 50 ng of RSV-β-galactosidase control plasmid. A portion of 0.1–5 μM of 17-DMAG was added as indicated for 16 h. (**b**) The expression levels of Tax, HSP90 and tubulin in 10 μg of lysates from panel (**a**) were monitored by IB with monoclonal antibodies for each protein.

β-globin intron II (pSG5-Tax),[24] whereas the other was driven by the HTLV-1-LTR (LTR-Tax). These lines were transfected with either a NF-κB-responsive or a HTLV-1-LTR luciferase reporter (Figures 3a and b and Figures 3c and d, respectively) and RSV-β-galactosidase for readout normalization. 17-DMAG treatment was found to suppress Tax-mediated NF-κB (Figures 3a, b and c) or HTLV-1-LTR activation (Figure 3d) regardless of whether Tax was expressed from pSG5-Tax (Figures 3a and b) or LTR-Tax (Figures 3c and d). In these experiments, the ectopically expressed Tax from transfected plasmid was again downregulated by 17-DMAG (Figure 3b). The same results were also obtained from the cell lysates transfected with LTR-Tax or CMV-Tax (data not shown). In addition to these two enhancers, activator protein 1 activation by Tax[34] was also inhibited by 17-DMAG (data not shown). As the three discrete pathways

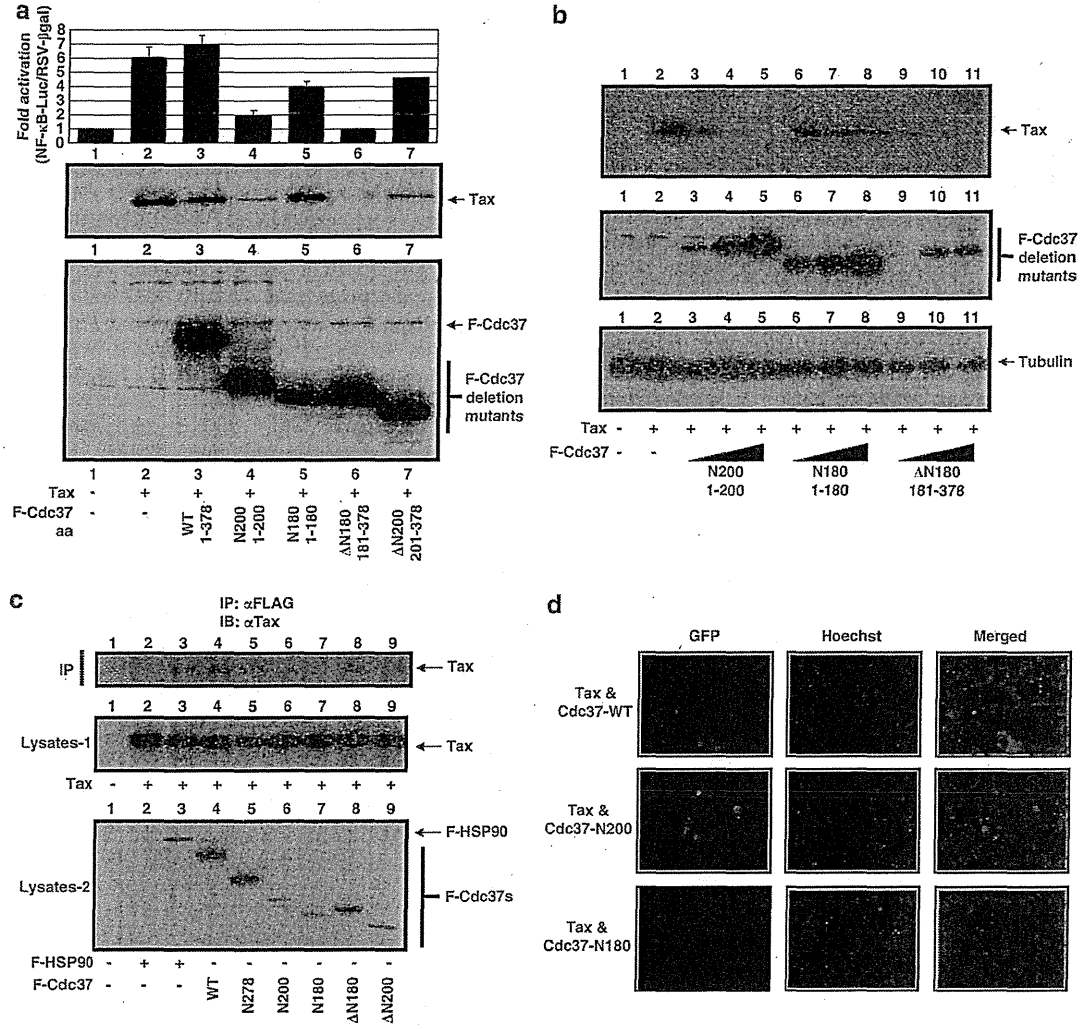

Figure 4. CBD of Cdc37 plays a crucial role for Tax stability in cells. (**a**) Co-transfection of LTR-Tax and pcDNA3-Flag-tagged Cdc37 (F-Cdc37) mutants. Lane 1: control pcDNA3 1 μg; lane 2: LTR-Tax 0.5 μg + pcDNA3 0.5 μg; lane 3: LTR-Tax 0.5 μg + F-Cdc37(1–378) wild type 0.5 μg; lane 4: LTR-Tax 0.5 μg + F-Cdc37(1–200) 0.5 μg; lane 5: LTR-Tax 0.5 μg + F-Cdc37(1–180) 0.5 μg; lane 6: LTR-Tax 0.5 μg + F-Cdc37(181–378) 0.5 μg; lane 7: LTR-Tax 0.5 μg + F-Cdc37(201–378) 0.5 μg. After 40 h transfection, HEK293 cells were lysed with 100 μl of lysis buffer, and the NF-κB-dependent luciferase activity was normalized with β-galactosidase value (upper panel). A portion of 10 μg of each lysate was resolved by sodium dodecyl sulfate-polyacrylamide gel electrophoresis, and the expression of Tax (middle panel) or Flag-tagged Cdc37s (lower panel) was detected by specific monoclonal antibodies. (**b**) Dose-dependent degradation of Tax by F-Cdc37 mutants. Lane 1: control pcDNA3 1 μg; lanes 2–11: 0.5 μg of LTR-Tax; lanes 3–5: plus 0.125, 0.25 and 0.5 μg of F-Cdc37(1–200); lanes 6–8: plus 0.125, 0.25 and 0.5 μg of F-Cdc37(1–180); lanes 9–11: plus 0.125, 0.25 and 0.5 μg of F-Cdc37(181–378). pcDNA3 was added to normalize the DNA amount. Tax (upper panel), Flag-tagged Cdc37s (middle panel) and tubulin (lower panel) were detected by specific monoclonal antibodies. (**c**) Cdc37's CBD (amino-acid residues 181–200(ref. 26)) is required for Tax interaction. A portion of 0.5 μg of control pcDNA3 (lane 1) or LTR-Tax (lanes 2–9) was transfected (lysate-1, middle panel) and 0.5 g of control pcDNA3 (lanes 1 and 2), F-HSP90 (lane 3), wild-type F-Cdc37(1–378, lane 4), F-Cdc37(1–278, lane 5), F-Cdc37(1–200, lane 6), F-Cdc37(1–180, lane 7), F-Cdc37(181–378, lane 8) and F-Cdc37(201–378, lane 9) were transfected separately (lysate-2, lower panel). The expression of each protein in cell lysates was detected by specific monoclonal antibodies (middle and bottom panels). A portion of 200 μg of each lane's cell lysates was mixed and subjected to Co-IP with 2 μg of rabbit anti-Flag antibodies, and each Co-IP complex was washed four times with Co-IP buffer, and following sodium dodecyl sulfate-polyacrylamide gel electrophoresis, Tax was detected by anti-Tax antibody (upper panel). (**d**) GFP two-hybrid binding assay between Cdc37 and Tax. HEK293 cells seeded on the six-well plates were transfected with phmKGN-MC-Tax and phmKGC-MN-Cdc37 or its mutant −Cdc37(N200) and −Cdc37(N180) by FugeneHD. After 48 h incubation, the transfected HEK293 cells were treated with Hoechst 34442 (Sigma) at the final concentration of 1 μM. Light and fluorescent (GFP and Hoechst 34442) microscopic observation and photography were performed by BZ-9000 Biorevo all-in-one fluorescence microscope (Keyence).

activated by Tax are inhibited by 17-DMAG treatment, the simplest interpretation suggests that all these effects arise from 17-DMAG-mediated destabilization of the Tax protein itself.

The client-binding domain of CDC37 plays crucial roles in Tax stabilization and Tax-mediated NF-κB activation

The molecular chaperone activity of HSP90 is usually exerted in cooperation with various co-chaperones. CDC37 was identified along with HSP90 as an essential component for a TNF-α-activated HMW-IKK complex.[12] As our current study shows the involvement of HSP90 in Tax-mediated HMW-IKK formation and NF-κB activation,[11,17] we generated Flag-tagged serial deletion mutants of HSP90 and CDC37 to examine their potential effects on Tax activity.

HSP90 has three distinct functional domains as described in Supplementary Figure 3.[35–37] We generated five deletion mutants, N, N+M, M, M+C and C, and transduced each with a Tax expression vector into HEK293 cells to determine any dominant-negative effects. Surprisingly, none of these mutants showed suppressive effects on Tax-mediated NF-κB activation or Tax stabilization (data not shown).

We then investigated the possible involvement of CDC37 in Tax stabilization and NF-κB signaling according to its functional domains (Supplementary Figure 3), namely, an HSP90-binding domain expanding through M164 to E221;[38] a kinase-binding domain at amino-acid residues 40–110;[39] a client-binding domain (CBD, amino-acid residues 181–200);[26] and a self-dimerization domain (amino-acid residues 240–260).[39] Although overexpression of full-length CDC37 slightly enhanced NF-κB activation (Figure 4a upper panel, lane 3), the mutants containing CBD, CDC37(1–200) and CDC37(181–378), strongly suppressed Tax-mediated NF-κB activation (Figure 4a upper panel, lanes 4 and 6) and induced extensive Tax degradation (Figure 4a middle panel, lanes 4 and 6). The mutants CDC37(1–180) and CDC37 (201–378) lacking CBD had little effects on either NF-κB activation or Tax stability (lanes 5 and 7). Tax degradation was reconfirmed by titration of these mutants (Figure 4b). Both CCD37(1–200) and CCD37 (181–378) progressively promoted Tax degradation (lanes 3–5 and 9–11, respectively), but CDC37(1–180) had little effects (lanes 6–8). Coexpression of certain sets of CDC37 mutants could promote Tax degradation through impaired physical interaction with Tax. We transfected HEK293 cells with Tax or Flag-CDC37 expression vectors separately to avoid spontaneous Tax degradation, and each cell lysate was mixed and applied for Co-IP experiments with anti-Flag antibodies (Figure 4c). Each protein expression was confirmed by immunoblotting for Tax (middle panel) or Flag (lower panel). Although the immunoprecipitates from wild-type HSP90 (upper panel, lane 3), CDC37 (lane 4) and Tax-degrading CDC37(1–200) and CDC37(181–378) (lanes 6 and 8) contained Tax in the complex, the immunoprecipitates from CDC37(1–180) and CDC37(201–378) lacking Tax-degrading properties did not (lanes 7 and 9).

Finally, we examined direct interaction between the two proteins using a GFP two-hybrid assay. Tax, tagged with the N-terminal portion of Kusabira-Green[27] fluorescent protein, and CDC37s (1–378, 1–200 and 1–180), tagged with the C-terminal portion, were co-transfected into HEK293 cells. Consistent with Co-IP results, co-transfectants of Tax and CDC37(1–378) or CDC37(1–200) emitted green fluorescence but Tax plus CDC37

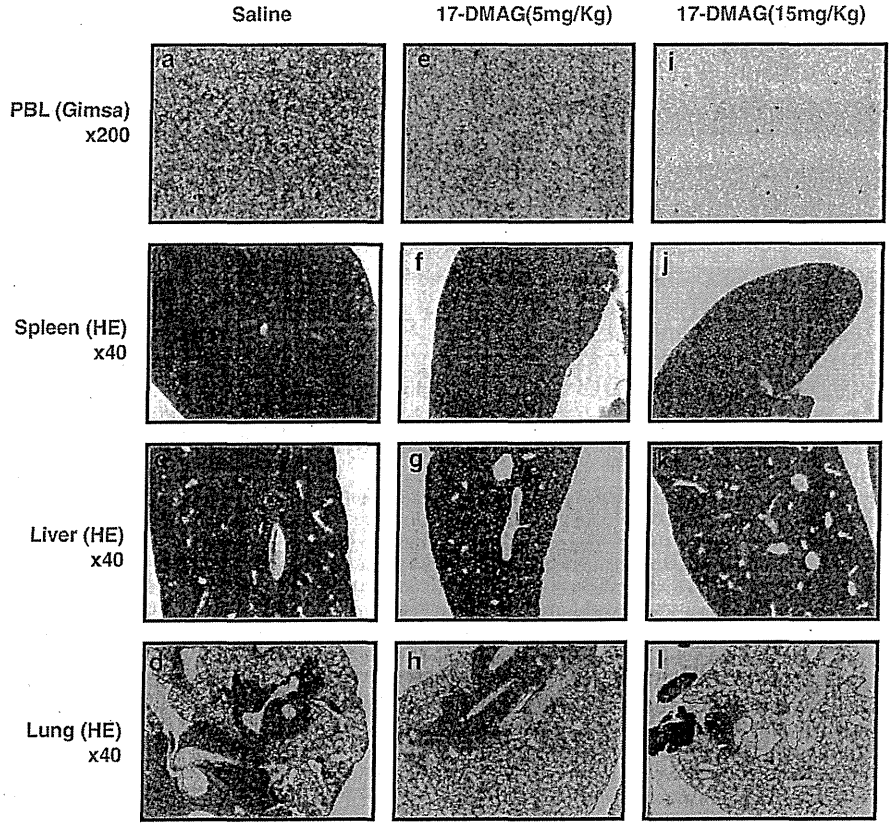

Figure 5. Oral administration of 17-DMAG blocks aggressive infiltration of Lck-Tax Tg cells into multiple organs of SCID mice. Two million Lck-Tax Tg cells were injected intraperitoneally into SCID mice. 17-DMAG was administered orally 5 days per week, with 5 mg/kg body weight (**e–h**) or 15 mg/kg body weight (**i–l**) or untreated (**a–d**). Mice were sacrificed after 21 days incubation, and organs were processed for Giemsa (**a, e, i**) or hematoxylin and eosin (HE, **b–d, f–h** and **j–l**) staining. Microscopic observations were performed and photographed with indicated magnifications. Tg, transgenic.